2018

Transcriptional characterization of osteogenic and adipogenic differentiation of human bone marrow derived mesenchymal stem cells in 2D and 3D peptide hydrogel culture system

R. M. Imtiaz Karim Rony
Wright State University

TRANSCRIPTIONAL CHARACTERIZATION OF OSTEOGENIC AND ADIPOGENIC DIFFERENTIATION OF HUMAN BONE MARROW DERIVED MESENCHYMAL STEM CELLS IN 2D AND 3D PEPTIDE HYDROGEL CULTURE SYSTEM.

A thesis submitted in partial fulfillment of the requirement for the degree of Master of Science

by

R M IMTIAZ KARIM RONY

B.S., Khulna University, Bangladesh, 2013.

2018

Wright State University.

WRIGHT STATE UNIVERSITY
GRADUATE SCHOOL

08/24/2018

I HEREBY RECOMMEND THAT THE THESIS PREPARED UNDER MY SUPERVISION BY R M Imtiaz Karim Rony ENTITLED Transcriptional characterization of osteogenic and adipogenic differentiation of human bone marrow derived mesenchymal stem cells in 2D and 3D peptide hydrogel culture system BE ACCEPTED IN PARTIAL FULFILLMENT OF THE REQUIREMENTS FOR THE DEGREE OF Master of Science.

Katherine Excoffon, PhD. Thesis Co-Director

Jaime E Ramirez-Vick, PhD. Thesis Co-Director

David L. Goldstein, Ph.D.
Chair, Department of Biological Sciences

Committee on Final Examination

Katherine Excoffon, PhD.

Jaime E Ramirez-Vick, PhD.

Barbara Hull, PhD.

Shulin Ju, PhD.

Barry Milligan, Ph.D.
Interim Dean of the Graduate School

Abstract

Rony, R M Imtiaz Karim. M.S. Department of Biological Sciences, Wright State University, 2018. Transcriptional characterization of osteogenic and adipogenic differentiation of human bone marrow derived mesenchymal stem cells in 2D and 3D peptide hydrogel culture system.

Mesenchymal stem cells (MSCs) are adult multipotent stem cell that can differentiate into mesodermal lineages such osteoblast, adipocytes, and chondrocytes, or can be transdifferentiated into clinically relevant lineages such as cardiac or neural cells using *in vitro* reprogramming techniques. In addition to the multilineage differentiation potential, MSCs from most tissue origins such bone marrow derived mesenchymal stem cells (BM-MSCs) or adipose derived mesenchymal stem cells (AD-MSCs) have immune modulatory functions which indicate their promise in clinical applications for cell-based therapy, tissue engineering, and regenerative medicine. In recent years, three-dimensional (3D) cell culture systems, which utilize 3D scaffolds or hydrogels to provide a physiological 3D microenvironment that mimics the native extracellular matrix, have been largely embraced to study cellular function and cell fate determination using different cell types. Although many investigators have shown that stem cell self-renewal/differentiation is modulated by the 3D scaffold chemistry and/or its surface topology, less attention has been given to undercover how such 3D scaffold affects chromatin organization and gene expression of key developmental regulators or lineage specifiers at the transcription and translation level during the course of stem cell differentiation. In this novel study, we have

established a Corning® PuraMatrix™ Peptide Hydrogel based 3D culture system for BM-MSCs and have analyzed key transcription factors regulating osteogenic (RUNX2, OSX, TWIST1) and adipogenic (PPARγ, C/EBPα, CHOP10) differentiation of BM-MSCs grown in a 2D culture and a PuraMatrix™ peptide hydrogel-based 3D culture. BM-MSCs adopt a completely different morphology and metabolism when encapsulated in PuraMatrix™ peptide hydrogel. Moreover, expression of these key osteogenic (RUNX2, OSX, TWIST1) and adipogenic (PPARγ, C/EBPα, CHOP10) transcription factors are differentially expressed between 2D and 3D culture system at different stages of BM-MSCS differentiation.

Table of Contents

Table of Contents (Continued)

List of Figures

List of Figures (Continued)

List of Figures (Continued)

List of Tables

List of Abbreviations

AD-MSCs	Adipose derived mesenchymal stem cells
BM-MSCs	Bone marrow derived mesenchymal stem
ESCs	Embryonic stem cells
HSCs	Hematopoietic stem cells
ICM	Inner cell mass
MSCs	Mesenchymal Stem Cells
NSCs	Neural stem cells
OSX (SP7)	Osterix
RUNX2(Cbfa-1)	Runt-domain containing transcription factor 2
TFs	Transcription Factors
PPARγ	Peroxisome proliferator-activated receptor gamma
TWIST1	Twist-related protein 1
C/EBPα	CCAAT/enhancer binding protein alpha
CHOP10 (DDIT3)	C/EBP homologous protein or DNA damage-inducible transcript 3
DLX3	Distal-Less Homeobox 3

List of Abbreviations (Continued)

DLX5	Distal-Less Homeobox 5
DLX6	Distal-Less Homeobox 3
C/EBPβ	CCAAT/enhancer binding protein beta
C/EBPδ	CCAAT/enhancer binding protein delta
ADD1	Adipocyte commitment and differentiation dependent factor 1
KLF5	Krüppel-like factor 5
TLE3	Transducin like enhancer of split 3
MSX2	Homeobox protein MSX-2
FOXC2	Forkhead box protein C2
BMP	Bone morphogenetic protein
LPL	Lipoprotein lipase
FAS	Fatty acid synthase
ECM	Extracellular matrix
MVEC	Human microvascular endothelial cells
UPR	Unfolded protein response
TBP	Tata binding protein

List of Abbreviations (Continued)

ROCK	Rho kinase
ERK1/2	Extracellular signal-regulated protein kinases 1 and 2

Acknowledgement

First of all, I would like to thank Dr. Jaime E Ramirez-Vick and Dr. Kate Excoffon at Wright State University without whom this study would not have been possible. I would also like to thank Dr. Barbara E Hull and Dr. Shulin Ju for their support and insightful remarks with regards to experimental design and other aspects of this study. I would also like to thank Dr. Puspendra Singh, Dr. Priyanka Sharma, Dr. David R. Ladle, and James Matthew Readler for their insightful suggestions and help with different experiments. I am also very grateful to my family for their consistent support and encourage. Finally, I am sincerely grateful to Dr. Jamie E Ramirez-Vick, Dr. Barbara Hull, and Dr. Kate Excoffon for their sincere patience and guidance with the writing process. This study is supported by Wright State University research funding.

Sincerely,

R M Imtiaz Karim Rony

Chapter 1: Introduction.

Stem cells are group of cells that can self-renew and specialize into different cell types, based on their differentiation potential or *potency*. In higher animals, embryonic stem cells (ESCs) from the inner cell mass (ICM) of the blastocyst stage embryo orchestrate early embryonic development and give rise to all functional cell types and tissues - a developmental potential known as *pluripotency* (Thomson et al., 1998; Nichols and Smith, 2012). During development, ESCs also give rise to certain tissue specific stem cells known as adult stem cells. Unlike pluripotent ESCs, adult stem cells such as hematopoietic stem cells (HSCs) or neural stem cells (NSCs) can only differentiate into certain lineages and have limited self-renewal ability, hence are characterized as *multipotent* (Gonzalez and Bernad, 2012). Nevertheless, the prime function of these adult stem cells is to replenish damage cells/tissues and maintain tissue homeostasis throughout the lifespan of an organism (Grandel et al., 2006; Wilson et al., 2008; Bonaguidi et al., 2011)

Mesenchymal stem cells (MSCs) are adult multipotent stem cells that can self-renew *in vitro*, and differentiate into mesodermal lineages (Pittenger et al., 1999). Typically, MSCs are characterized as plastic adherent, spindle shaped stromal cells that have fibroblast like morphology (Pittenger et al., 1999). Bone marrow has long been considered as the key source of MSCs; however, multipotent MSCs or MSC-like cells have also been isolated from different adult tissues such as skeletal muscle, adipose tissue,

umbilical cord, amniotic fluid, peripheral blood, dental pulp, etc. (da Silva Meirelles et al., 2006). Typically, MSCs or MSCs like cell populations from adult tissues show considerable heterogenicity in terms of cell surface markers and gene expression profile (Panepucci et al., 2004; Kaltz et al., 2010). To minimize complexities associated with characterizing true multipotent MSCs populations, the *International Society for Cellular Therapy* has proposed defined criteria for characterizing multipotent MSCs. These includes (1) adherence to plastic in standard culture condition, (2) expression of positive ($\geq 95\%^{+}$) marker CD105, CD73, CD90 while being negative ($\leq 2\%+$) for CD45, CD34, CD14 or CD11b, CD79a or CD19, HLA-DR, and (3) *in vitro* differentiation into osteoblasts, adipocytes, chondroblasts (Dominici et al., 2006). In addition to musculoskeletal tissues, MSCs can differentiate or transdifferentiate into other lineages such as cardiac cells, neuronal cells, hepatic cells (Figure 1) (Xu et al., 2004; Tao et al., 2005; Chivu et al., 2009).

In general, MSCs residing in the adult tissues or stem cell niches (e.g. HSCs/niches) maintain tissue homeostasis by two mechanisms. MSCs either undergo differentiation to generate functional cells for replenishing damaged cells/tissues or MSCs secrete a variety of cytokines and growth factors termed *trophic factors* that regulate the growth and functionality of surrounding cells or stem cell populations (Uccelli et al., 2008). MSCs in the bone marrow niche support hematopoietic stem cells (HSCs) self-renewal/quiescence and prevents their differentiation, either through direct physical interaction or by secreting array of cytokines/chemokines (Oostendorp et al., 2002; Calvi et al., 2003; Mendez-Ferrer et al., 2010; Omatsu et al., 2010). BM-MSCs also prevent niche HSCs from undergoing apoptosis and helps maintain a constant physiological reservoir of HSCs (Wilson and Trumpp, 2006; Wilson et al., 2008).

Another key feature of MSCs is that they can modulate the host immune system and avoid immune rejection. Both *in vitro* and *in vivo* studies have found that allogenic or autologous transplantation of MSCs suppress CD4(+) and CD8(+) T cell function and proliferation (Di Nicola et al., 2002), inhibit dendritic cells maturation and antigen presentation function (Nauta et al., 2006), and suppress B cell proliferation by arresting cell cycle (Corcione et al., 2006).

Owing to their multilineage differentiation and immunomodulatory potential, MSCs have become a very promising resource for regenerative medicine and tissue engineering. Many preclinical and clinical studies are now underway, exploring therapeutic potential of MSCs for the treatment of autoimmune or inflammatory diseases such as Crohn's disease or Graft-versus-host disease (Le Blanc and Mougiakakos, 2012). MSCs are also prime candidates for bone disorders, cartilage and intervertebral disc repair, and hold great promise for treating ischemic cardiac disease, pulmonary fibrosis, and acute renal failure (Kariminekoo et al., 2016). In addition to direct allogenic transplantation, MSCs are now being extensively studied for *in vitro* tissue engineering. Using chemically defined 3D hydrogels or scaffolds for structural and mechanical support, MSCs can be expanded for direct differentiation into complex tissue structure such as bone, cartilage, or skeletal muscle (Zhang et al., 2015; Adamzyk et al., 2016; Witt et al., 2017).

Despite such potential therapeutic/translational advancements in MSCs biology, the molecular mechanisms underlying MSCs differentiation and lineage specification is poorly understood. In particular, how MSCs maintain a balance between osteogenesis and adipogenesis has always been of great interest since any shift in this balance is associated with aging (Moerman et al., 2004), obesity (Bredella et al., 2011), and diseases such as

osteoporosis (Justesen et al., 2001). Although the key transcription factors (TFs) and signaling pathways regulating osteogenesis and adipogenesis in MSCs have been characterized (Chen et al., 2016), how these factors are coregulated at each stage of differentiation, at both transcriptional and translational level, is still being investigated. Also, there is considerable interest in characterizing MSC differentiation, particularly the transcriptional and epigenetic changes accompanying differentiation in 3D culture systems such as hydrogels or scaffolds, since these matrices mimic the *in vivo* microenvironment. With these prospects in mind, in this project we aim at profiling the expression of key TFs regulating osteogenic and adipogenic differentiation of human bone marrow derived mesenchymal stem cells (BM-MSCs) at transcriptional and translational level, using 2D (monolayer) and self-assembled peptide hydrogel-based 3D culture system (PuraMatrix™). Previous studies showed that TFs RUNX2, Osterix (Osx), DLX3, DLX5, DLX6, MSX2, FOXC2, TWIST, and PPARγ, C/EBPα, C/EBPβ, C/EBPδ, ADD1, KLF5, TLE3, and CHOP10 are the key regulators and play a critical role at different stages of osteogenic and adipogenic differentiation of MSCs, respectively (Zhang et al., 2012). Therefore, we sought to quantify the mRNA and protein levels of these osteogenic and adipogenic TFs, at different time points during BM-MSCs differentiation in 2D and 3D culture systems and distinguish how dimensionality modulates their differentiation and gene expression pattern. Our experiments have uncovered new insights into the dynamics of transcriptional regulation underlying osteogenesis and adipogenesis of BM-MSCs, specifically how gene expression pattern of key TFs change during the course of differentiation, and between 2D and 3D culture systems.

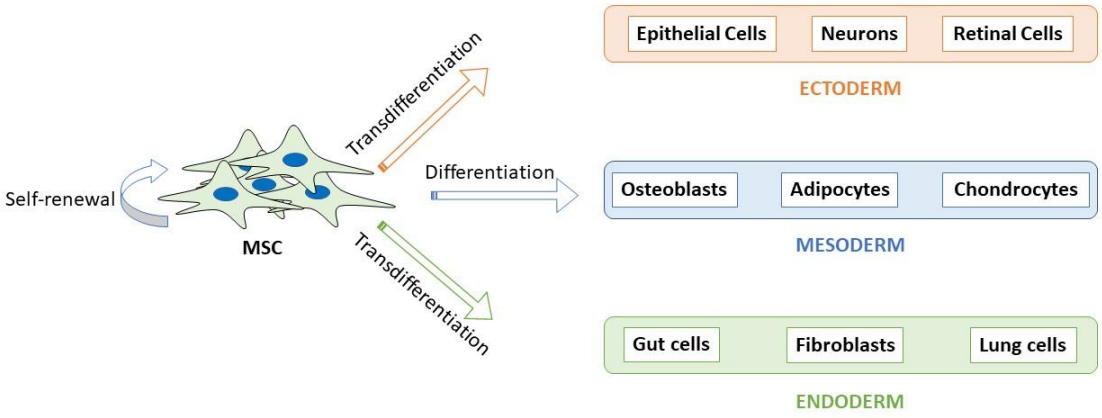

Figure 1: Multipotency of mesenchymal stem cells (MSCs). MSCs can self-renew to produce more MSCs or can differentiation into mesodermal lineages such as adipocytes, osteoblasts, or chondrocytes. MSCs can also transdifferentiate into other lineages within ectoderm or endoderm.

Chapter 2: Background

2.1 Bone marrow and adipose derived mesenchymal stem cells:

Bone marrow (BM-MSCs) and adipose derived MSCs (AD-MSCs) are the most extensively investigated multipotent MSCs owing to their availability and ease of isolation. Both of these cell types, irrespective of their tissue origin, show fibroblast morphology, express typical MSCs markers (positive for CD29, CD44, CD105, CD166 while being negative for CD14, CD45), and can differentiate into osteogenic, adipogenic, and chondrogenic lineages (Lee et al., 2004; Peng et al., 2008).

However, reports suggest that there are some inherent differences between BM-MSCs and AD-MSCs (Zuk et al., 2002; De Ugarte et al., 2003; Lee et al., 2004; Peng et al., 2008). Morphologically, BM-MSCs colonies have been found to be slightly bigger than AD-MSCs although AD-MSCs possess higher proliferative ability (Figure.2) (Lee et al., 2004; Peng et al., 2008). In contrast, AD-MSCs have higher resistance towards serum deprivation-induced apoptosis (Peng et al., 2008), and higher immunomodulatory potential than BM-MSCs (Dominici et al., 2006). Only AD-MSCs are positive for CD49d, CD54, CD34, CD106, and CD49d whereas the expression of CD106 is only detected in BM-MSCs (Zuk et al., 2002; De Ugarte et al., 2003). Some cytokines are also thought to be differentially expressed, due to their difference in tissue specificity (Li et al., 2015). Regardless of these similarities and differences, most of the key transcription factors (e.g.

RUNX2, PPARγ, etc.) and their regulatory mechanisms underlying MSCs self-renewal and differentiation are expected to be similar in both cell types.

2.2 Transcriptional Regulations of mesenchymal stem cells osteogenesis and adipogenesis:

Previous studies have established that differentiation of MSCs is governed by a transcriptional network comprised of core TFs, cofactors, signaling pathways, and other regulators such as non-coding RNA (miRNA, lncRNA) and chromatin modifiers that act in concert to specify osteogenic, adipogenic, or chondrogenic specialization (Guo et al., 2011; Zhang et al., 2012; Saidi et al., 2017).

For osteogenic differentiation of MSCs, TF Runx2 (Zheng et al., 2004), Osx (Nakashima et al., 2002), Dlx3 (Hassan et al., 2004), Dlx5 (Ryoo et al., 1997) (Shirakabe et al., 2001), Dlx6 (Li et al., 2008), Msx2 (Cheng et al., 2003), Foxc2 (Kim et al., 2009), and Twist (Hayashi et al., 2007) appear to play a crucial role.

Runx2, also known as Cbfa-1 (core binding factor α 1), is a runt-domain containing TF, considered to be the master regulator of osteogenesis. Runx2 is expressed early during skeleton formation in the developing embryo (Ducy et al., 1997) and Runx2 null mice immediately die after birth due to a complete lack of bone formation (Komori et al., 1997). Forced expression of Runx2 in preosteoblast cells results in increased expression of osteoblast specific genes such as osteopontin, type-I collagen, and participate in differentiation of MSCs into osteoblast like cells, both *in vitro* and *in vivo* (Ducy et al., 1997; Zheng et al., 2004). In addition to specifying osteogenic fate, Runx2 inhibits

chondrogenic and adipogenic differentiation of MSCs, which corroborates Runx2's cardinal function in osteogenesis (Kobayashi et al., 2000).

On the other hand, Osx is a zinc finger containing TF, exclusively expressed in developing bones (Nakashima et al., 2002). Osx is essential for osteoblast differentiation since Osx null mice exhibit normal physical morphology but lack bone formation (Nakashima et al., 2002). Interestingly, Osx is a downstream regulator of Runx2 and Osx expression is regulated by Runx2 (Nakashima et al., 2002). It has been proposed that Runx2 expression differentiates MSCs into bipotential preosteoblast progenitors that can differentiate into osteoblast and chondrocytes (Nakashima et al., 2002). Osx expression then direct the differentiation towards functional osteoblasts (Nakashima et al., 2002). In fact, ectopic expression of Osx alone promotes osteogenic differentiation in MSCs (Wu et al., 2007). However, Osx cannot induce terminal differentiation on its own, other regulators are needed as well (Kurata et al., 2007).

Dlx3, 5, and 6 are homeodomain TFs that have been implicated in embryonic bone formation and osteoblast differentiation (Zhao et al., 1994; Hassan et al., 2004; Li et al., 2008). Dlx3 is highly expressed in osteoblasts and forced expression of Dlx3 in osteoprogenitor cells induces expression of osteogenic genes (Hassan et al., 2004). Both Dlx5 and Dlx6 are essential for craniofacial, axial, and appendicular skeletal development and their ablation leads to postnatal lethality (Robledo et al., 2002). Just like Dlx3, overexpression of Dlx5 accelerates osteoblast differentiation and stimulates increased mineralization in preosteoblasts (Tadic et al., 2002). Interestingly, both Dlx3 and Dlx5 induce osteogenic differentiation by activating Runx2 expression (Hassan et al., 2006). Overexpression of Dlx6 also strongly induces osteoblast differentiation (Li et al., 2008).

Interestingly, Dlx5 and Dlx6 are preferentially expressed in immature osteoblasts whereas Dlx3 is highly expressed in differentiated osteoblast and osteocytes (Ryoo et al., 1997; Li et al., 2008).

Msx2 is another homeobox TF of the Msx gene family that regulates osteogenesis (Dodig et al., 1999). Induction of Msx2 expression in MSCs leads to osteogenic differentiation, marked by significantly increased alkaline phosphatase activity and calcification in the osteoblasts (Ichida et al., 2004). Msx2 expression also inhibits adipogenesis by repressing key adipogenic TFs such as PPARγ, C/EBPα, C/EBPβ, or C/EBPδ (Cheng et al., 2003; Ichida et al., 2004).

Foxc2, a member of the forkhead/winged helix TF family, also modulates osteogenic differentiation of MSCs (Kim et al., 2009). Ectopic expression of Foxc2 induces osteoblast differentiation in MSCs and preosteoblast cells by upregulating integrin β1, which in turn improves osteoblast proliferation and differentiation (Park et al., 2011).

Twist is a basic helix-loop-helix (bHLH) TF which negatively regulates MSCs osteogenesis (Hayashi et al., 2007). Twist overexpression inhibits bone morphogenetic protein (BMP) signaling induced osteogenic differentiation of MSCs (Hayashi et al., 2007). Twist repressive function depends on direct interaction and formation of multiprotein repressive complex with Smad4 and histone deacetylase (HDAC) (Hayashi et al., 2007).

In contrast, adipogenic differentiation of MSCs is regulated by a combination of TFs PPARγ (Tontonoz et al., 1994), C/EBPα (Rosen et al., 2002), C/EBPβ (Hamm et al., 2001), C/EBPδ (Hishida et al., 2009), ADD1/SREBP1 (Tontonoz et al., 1993), KLF5 (Oishi et al., 2005), TLE3 (Kokabu et al., 2013), and CHOP10 (Batchvarova et al., 1995).

Peroxisome proliferator activated receptor-γ (PPARγ), a nuclear hormone receptor, is the master regulator of adipogenesis. PPARγ, particularly PPARγ2 is highly expressed in adipocyte and forced expression PPARγ2 induces adipose differentiation in cultured fibroblasts (Tontonoz et al., 1994) and transdifferentiate of myoblasts into adipocytes (Hu et al., 1995). Ectopic PPARγ expression upregulates adipogenesis associated genes as well as genes for fatty acid transporter, adipocyte lipid-binding protein (Bastie et al., 1999).

CAAT/enhancer binding proteins (C/EBPs) are another group of TFs that regulate adipogenesis. These are highly expressed in liver and adipose tissue. Forced expression of C/EBPs, particularly C/EBPβ stimulates adipogenic differentiation in multipotent MSCs (Wu et al., 1995). C/EBPβ plays the key role during adipogenesis. Ectopic expression of C/EBPβ in MSCs upregulates PPARγ which in turns stimulates expression of other adipogenic factors (Hamm et al., 2001). Both C/EBPβ and C/EBPδ are typically expressed early during preadipocyte differentiation (Tang et al., 2004). C/EBPβ then activates C/EBPα and PPARγ. C/EBPα then induces terminal differentiation and maturation of adipocytes by stimulating adipocyte-specific proteins (Tang et al., 2004; Hishida et al., 2009).

Adipocyte commitment and differentiation dependent factor 1 (ADD1), also known as sterol regulatory element-binding protein 1 (SREBP1) is a pro-adipogenic bHLH containing TF that plays a key role during early adipogenic differentiation (Tontonoz et al., 1993). Ectopic expression of ADD1 induces adipogenic differentiation in non-adipogenic NIH3T3 cells and activates genes associated with fatty acid metabolism such as fatty acid synthase (FAS) and lipoprotein lipase (LPL) (Kim and Spiegelman, 1996).

ADD1/SREBP1 modulate adipogenesis by directing upregulate PPARγ expression (Fajas et al., 1999)

Another zinc-finger TF associated with adipogenesis is Krüppel-like factor 5 (KLF5). KLF5 knockout mice are devoid of adipose tissues while forced expression of KLF5 in MSCs induces adipogenic differentiation without other differentiation inducing supplements (Oishi et al., 2005). KLF5 is typically activated early during adipocyte differentiation, and its expression is highest during pre-adipocyte to adipocyte differentiation (Oishi et al., 2005) (Mori et al., 2005). KLF5's key function in inducing adipogenesis is to upregulate PPARγ expression, which in turns coordinates terminal differentiation of adipocytes (Mori et al., 2005).

Transducin like enhancer of split 3 (TLE3) is a dual functionality transcriptional corepressor that also regulates adipogenesis. TLE3 promotes PPARγ expression and assists PPARγ in transcriptional activation of adipogenic genes (Villanueva et al., 2011). Meanwhile TLE3 inactivates Wnt signaling during adipogenesis by inhibiting TCL4 activation by b-catenin and prevents β-catenin dependent repression of adipocyte gene expression (Villanueva et al., 2011).

CHOP10 (Gadd153) is a nuclear protein which negatively regulates adipogenesis. At early stages of adipogenic differentiation, CHOP10 is expressed at an elevated level, heterodimerizes with C/EBPα or C/EBPβ and prevents their transcriptional activity (Batchvarova et al., 1995). However, at a later stage, when preadipocytes shift to S phase, CHOP10 expression is repressed and C/EBPα or C/EBPβ is released from CHOP10-mediated sequestration to transactivate adipogenic genes (Tang and Lane, 2000).

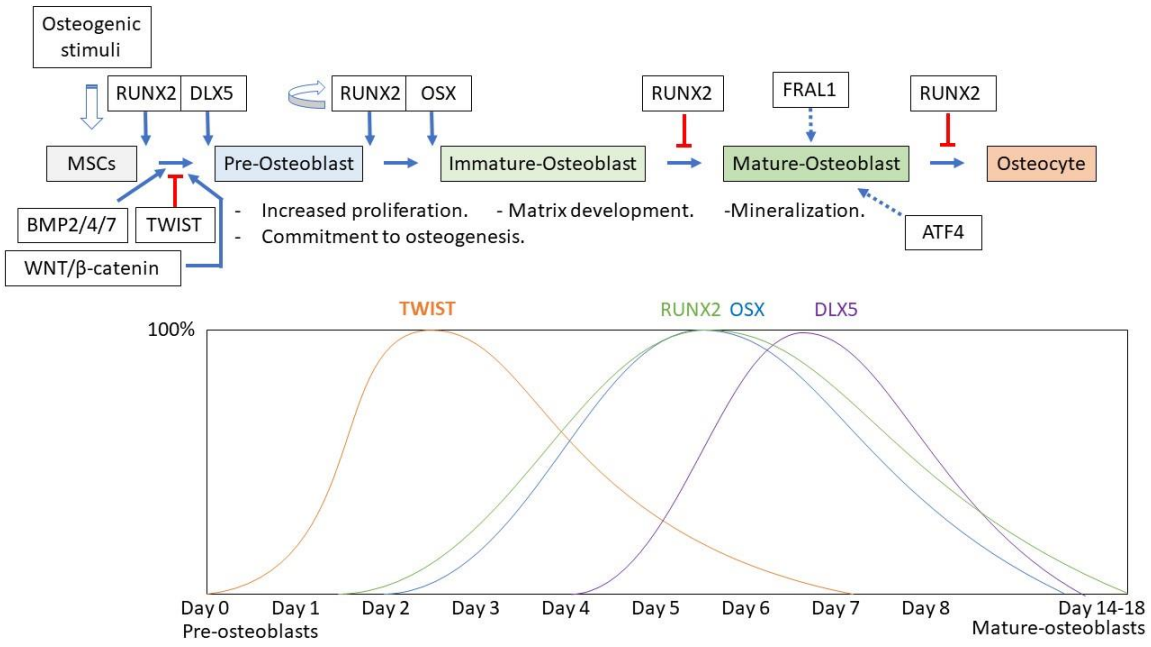

Figure 2: Lineage pathway of osteogenic differentiation of mesenchymal stem cells (MSCs). In response to osteogenic stimuli, MSCs differentiates into pre-osteoblast. Preosteoblast then undergo a series of morphological and of epigenetic/transcriptional remodeling governed by the key osteogenic transcription Factor, RUNX2, OSX, DLX5and becomes terminally differentiated into osteoblasts and osteoclasts, respectively. Expression of Runx2, Osx, Dlx5 and other osteogenic transcription factors is dynamically regulated at different stages of differentiation (Kobayashi et al., 2000; Nakashima et al., 2002; Tadic et al., 2002; Hassan et al., 2004; Hassan et al., 2006; Hayashi et al., 2007; Kurata et al., 2007; Li et al., 2008; Karsenty et al., 2009; Javed et al., 2010; Fakhry et al., 2013; Bruderer et al., 2014).

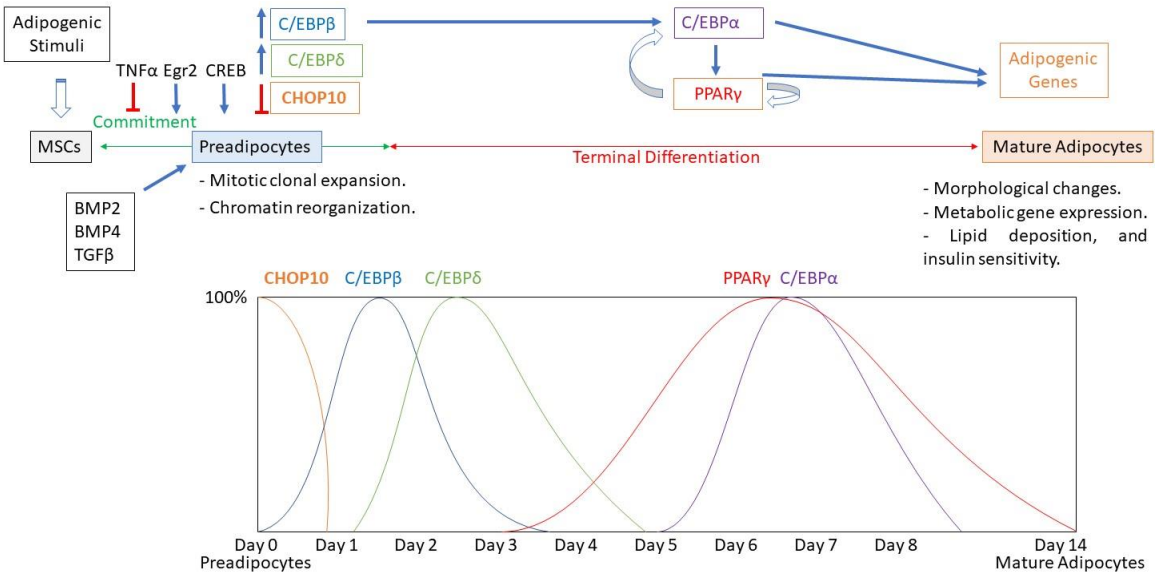

Figure 3: Lineage pathway of adipogenic differentiation of mesenchymal stem cells (MSCs) commence with MSC receiving adipogenic stimuli which induced adipogenic commitment to the MSCs and differentiation to preadipocytes. Preadipocytes then undergo terminal differentiation into mature adipocyte through a cascade of epigenetic and transcriptional regulation, mainly governed by key adipogenic transcription Factor, PPARγ, C/EBPα, C/EBPβ (Tontonoz et al., 1994; Batchvarova et al., 1995; Wu et al., 1995; Tang and Lane, 2000; Hamm et al., 2001; Rosen et al., 2002; Tang et al., 2004; Farmer, 2006; Rosen and MacDougald, 2006; Hishida et al., 2009; Cristancho and Lazar, 2011; Tang and Lane, 2012; Mota de Sa et al., 2017).

2.3 Cellular microenvironment, and 3D cell culture:

Historically, most aspects of cellular structure, function, and differentiation have been investigated using conventional 2D culture system – growing cells as a monolayer on cell culture plates/dishes (plastic/glass). Such 2D approach has largely been instrumental in uncovering fundamental basis of key cellular mechanisms such as replication, cell division, cell cycle, cell fate determination etc. However, cellular activities such as cell-extracellular matrix (ECM) interaction, cell fate determination due to cell-ECM interaction, cell-cell interaction in stem cell niche or tumor, or cellular microenvironment regulating gene expression or chromatin organization is very difficult to recapitulate in 2D culture system, due to the intrinsic property of two dimension (Duval et al., 2017). To overcome these hurdles, engineered scaffold or hydrogels that provides a 3D microenvironment to the cells and closely mimic extracellular matrix have been designed using natural or synthetic polymers that are either physically or chemically crosslinked (Tibbitt and Anseth, 2009). Typically, the formulation of many hydrogels requires incorporation of some natural extracellular matrix components such as laminin or collagen in addition to the polymers (Matrigel); however, there are hydrogels that are solely comprised of polymer or synthetic peptide (PuraMatrix). In addition to providing a 3D microenvironment for the cells, hydrogels are biocompatible, highly permeable to oxygen, nutrients, growth factors and supplement, able to exchange gas, and provide mechanical support to the encapsulated cells (Tibbitt and Anseth, 2009; Youngblood et al., 2018).

Accumulating evidence suggest that cell's behavior drastically changes when they are maintained in 3D culture system, marked by changes in cell morphology, viability, proliferation and differentiation potential, gene expression pattern etc., largely owing to

the 3D microenvironment that allow cells to respond to biophysical and mechanical stimuli as well the opportunity to interact with the extracellular matrix in all three dimensions, as *in vivo* (Baker and Chen, 2012; Gauvin et al., 2012; Bonnier et al., 2015; Vining and Mooney, 2017).

In addition to the 3D microenvironment provided by these hydrogels that allows encapsulated cells to adapt to different morphology/geometric shape and function, chemical/structural formulation of these 3D hydrogels as well as their intrinsic surface topographies also affect cell function and/or differentiation. For instance, both Engler et al., (2006) and Huebsch et al., (2010) have shown that MSCs preferentially undergo osteogenesis when the stiffness of the hydrogel is intermediate to rigid whereas soft matrices favor neurogenic commitment (Engler et al., 2006; Huebsch et al., 2010). Together these observations suggest that compared to 2D culture system, 3D culture system provides a more convenient and *in vivo*-like approach for studying cellular behavior and cell fate commitment.

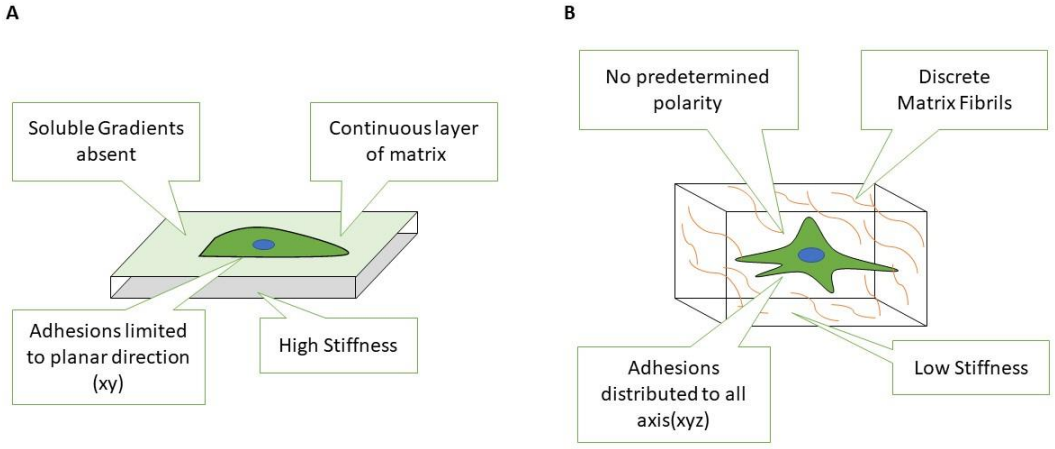

Figure 4: Adhesive, topographical, mechanical, and soluble cues in 2D and 3D culture system.

2.4 Corning® PuraMatrix™ Peptide Hydrogel system for 3D cell culturing:

Corning® PuraMatrix™ Peptide Hydrogel is a peptide based synthetic matrix, consisting of 1% (w/v) standard amino acids and 99% water. The structural basis of this peptide hydrogel is the RAD16 oligopeptide, which consists of arginine (R), alanine (A), and aspartic acid (D). Structurally RAD16 resembles the RGD (Arg-Gly-Asp) motif found in many extracellular matrix proteins such as fibronectin. The RGD motif is recognized by many proteins of the integrin family and this sequence has been found to play a crucial role in cell adhesion (Ruoslahti, 1996).

Being composed of alternative hydrophilic and hydrophobic amino acids, these peptides organize into β sheets in water (Zhang et al., 1995). In presence of physiological buffer or medium containing millimolar amount of salts, this peptide spontaneously organizes into membranous 3D matrices, exhibiting fibrous structure with average pore size of 50-200 nm (Zhang et al., 1995; Holmes et al., 2000). Key advantages of Corning® PuraMatrix™ Peptide Hydrogel over other hydrogels or 3D matrices such as Matrigel are that PuraMatrix is completely synthetic, can be produced in larger quantities, biocompatible, does not elicit immune response, and is devoid of animal products and pathogens.

To this end, multiple stem/progenitor/primary cell types such as neural stem cells (NSCs), and endothelial cells been used studied with Corning® PuraMatrix™ Peptide Hydrogel (Narmoneva et al., 2005; Koutsopoulos and Zhang, 2013). However, MSCs have not been studied with Corning® PuraMatrix™ Peptide Hydrogel yet. Therefore, one of the aims of this study was to characterize BM-MSCs encapsulation, viability and differentiation in Corning® PuraMatrix™ Peptide Hydrogel based 3D culture system.

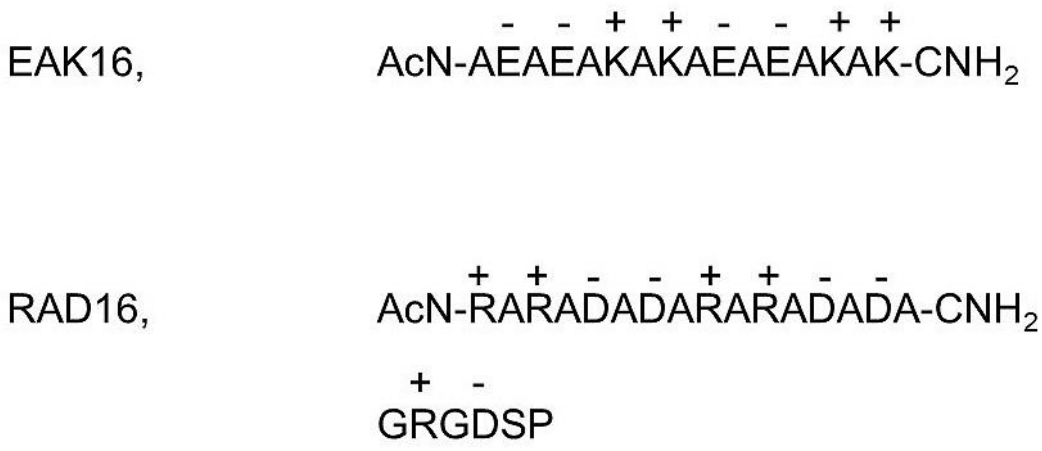

Figure 5: Structure of RAD16, and EAK16 oligopeptides. Here, A represents alanine; E = glutamic acid; K is lysine; R stands for arginine; D is aspartic acid; G = glycine; S is serine; P is proline. N- and C-termini end of the peptides is referred as N- and C-, - and + refer to the negatively and positively charged amino acids, respectively.

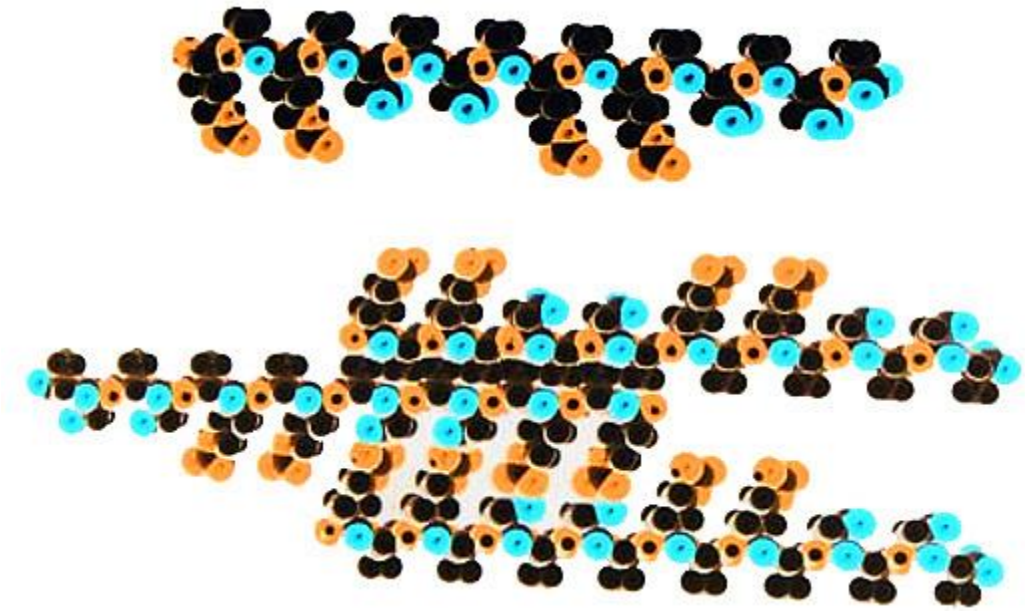

Figure 6: Proposed molecular model of the RAD16-II peptide which forms a stable β-strand with distinct polar and nonpolar sides in water or any other physiological solution (Top). Molecular model depicting suggested interpeptide interaction due to the self-complementary feature of RAD16 (Bottom). Adopted from (Holmes et al., 2000).

Chapter 3: Materials and Methods

3.1 Cell Culture:

Cryopreserved, passage 2 human bone-marrow derived mesenchymal stem cells (BM-MSCs), collected from healthy, non-diabetic donors, were purchased from Lonza (Catalog # PT-2501). These BM-MSCs express MSC-specific cell surface markers and can differentiate into osteogenic, adipogenic, and chondrogenic lineages, corroborating bona fide multipotency.

For experiments, BM-MSCs were seeded into T75 flasks at a density of 6,000 cells/cm^2 using MSCs growth medium (500ml of basal medium supplemented with 25 ml of fetal bovine serum, 5ml MSCs growth supplement, and 5ml penicillin/streptomycin solution) from ScienCell Research Laboratories (# 7501), at a rate of 0.2ml/cm^2 (i.e., 15ml for T75 flask). At 80-90% confluency, BM-MSCs were sub-cultured using manufacture's protocol. MSCs growth medium were removed from the culture flasks and the cells were washed with equal amount of PBS ($Ca^{2+}$and Mg^{2+} free). After aspirating the PBS from the flasks, adherent BM-MSCs were trypsinized using trypsin/EDTA solution (Lonza, # CC-3232) at a concentration of 0.05ml/cm^2 (i.e., 4ml per T75 flask) and the flasks were incubated at 37°C for 5 minutes in a humidified 5% CO_2 atmosphere. When ~ 90% of the cells detached from the flask's surface, the trypsin solution was neutralized with an equal volume of MSC growth medium. The trypsinized cells were transferred to 15ml centrifuge tubes and centrifuged for 5 minutes at 600 g. The supernatants were discarded, and the cell

pellets were re-suspended in 1ml MSC growth medium. After calculating the cell concentration, these were reseeded into new T75 flasks at the desired concentration and were sub-cultured until passage 4. All experiments were done using passage 4 BM-MSCs, unless mentioned otherwise.

3.2 3D Cell Culture with PuraMatrix Hydrogel:

3.2.1 BM-MSCs encapsulation in PuraMatrix Hydrogel:

For 3D cell cultures, BM-MSCs were encapsulated in Corning® PuraMatrix™ peptide hydrogel (Corning, # 354250) according to manufacturer's instruction, optimized accordingly.

The PuraMatrix hydrogel consists of 1% standard amino acids and 99% water. Although a range of PuraMatrix hydrogel concentrations (i.e., 0.125% - 1%) have been tested with BM-MSCs and adipose-derived MSCs, in our lab BM-MSCs appeared to be more resilient and adaptable to 0.125% and 0.25% hydrogels, with 0.125% allowing the most physiological adaptation and reorganization of the BM-MSCs within the matrix, based on microscopic analysis. Therefore, all the biochemical, and histological experiments were done with BM-MSCs encapsulated in 0.125% hydrogel unless mentioned otherwise.

To encapsulate BM-MSCs in 0.125% hydrogel, the hydrogel stock solution (1%) was sonicated in an ultrasonic bath for 30 minutes, to reduce its viscosity, and was diluted to 2× concentration of 0.125% hydrogel solution with 20% sucrose. Meanwhile, passage 4 BM-MSCs were trypsinized and re-suspended in 10% sucrose solution at a concentration of 1×10^6 cells/ml. Afterwards, the 2× concentrated 0.125% hydrogel solution were added

to individual 1.5ml centrifuge tubes (125µL for 24-well plates and 25 µL for 96-well plates) and an equal amount of cell-sucrose solution was mixed by gently pipetting up-and-down, followed by immediate plating into individual wells of non-treated cell culture plates. Gelation of the hydrogel was induced immediately by gently adding MSC growth medium in the corresponding wells. To neutralize the pH of the hydrogel with that of MSC medium, the medium was changed twice within one hour of cell encapsulation. Medium was changed every two days.

3.2.2 Cell recovery from 3D PuraMatrix Hydrogel for biochemical assays:

To recover BM-MSCs encapsulated 3D PuraMatrix hydrogel for biochemical assays, the hydrogels were mechanically disintegrated by repeated up-and-down pipetting inside the wells of the multi-well plate, followed by transfer of the hydrogel-medium mixtures to 15ml centrifuge tubes. The 3D culture wells were washed again with an equal volume of PBS (500µl/well for 24-well plates) and transferred to corresponding 15ml tubes. The PBS-matrix-medium mixtures were centrifuged at 1000g for 5 minutes at 4°C. The supernatants were discarded, with the remaining pellets consisting of cells and PuraMatrix peptide fragments. The pellets were washed by re-dissolving in 2ml PBS and centrifuged at 1000g for 5 minutes to re-pellet. These were resuspended in 500µl of Trypsin/EDTA and incubated at 37°C for 5 minutes in a humidified 5% CO_2 atmosphere. Afterwards, 2ml of MSCs growth media was added to neutralize the trypsin, and the mixture was centrifuged at 1000g for 5 minutes to re-pellet. The supernatants were discarded, and the pellets were re-dissolved in 500µl PBS by repeated up-and-down pipetting. The solutions were centrifuged, and the cells were collected as a pellet, that might retain some residual peptide fragments which should not interfere with downstream

applications. Total RNA and protein extract were prepared from the cell pellets using Trizol and RIPA buffer protocols mentioned for 2D cultured cells, described below.

3.3 Differentiation:

For differentiation experiments in 2D culture, passage 4 BM-MSCs were seeded into 12-well plates (triplicates for each condition: control, osteogenesis, and adipogenesis) at a density of 6,250 cells/cm^2, maintained in MSC growth medium (1ml per well). At ~90% confluency, osteogenic and adipogenic differentiation were induced by changing MSCs growth medium to osteogenic and adipogenic induction media, respectively. Osteogenic induction medium consists of MSCs growth medium supplemented with 0.1 µM dexamethasone, 0.2 mM l-ascorbate, and 10 mM glycerol-3-phosphate whereas adipogenic medium contains 1 µM dexamethasone, 0.5 mM 3-isobutyl-1-methylxanthine (IBMX), 100 µM indomethacin, and 10 µg/ml insulin supplemented in MSCs growth medium. For control, cells were maintained in MSCs growth medium only. All media were changed every 3-4 days.

For differentiation experiments in 3D hydrogel, 1×10^6 cells/ml passage 4 BM-MSCs were encapsulated in 0.125% PuraMatrix hydrogel and were seeded in 24-well un-treated plates. After 3 days post-encapsulation, to allow cells to adapt and reorganize within the hydrogel matrix, differentiation was induced by changing the MSCs growth medium to osteogenic and adipogenic induction media. The media were replaced every 2 days.

3.4 Staining:

3.4.1 Alizarin Red S Staining

Osteogenic differentiation of MSCs is characterized by deposition of calcium in pre/mature osteoblasts. Alizarin Red S staining is typically used to visualize calcium deposits following osteogenic differentiation, through the complexation of this dye with the calcium molecules via its sulfonic acid and/or hydroxy groups (Birmingham et al., 2012; Kraus et al., 2016).

For Alizarin Red S Staining, passage 4 BM-MSCs were grown on glass coverslips placed in 12-well plates in 2D cultures or 8-well chamber slides for 3D encapsulation. After medium aspiration, the cells were washed twice with PBS and fixed with 4% paraformaldehyde in PBS for 15 minutes at room temperature. The fixative was then removed, and the cells were washed 3 times with de-ionized (DI) H_2O. Afterwards, 1ml of Alizarin Red S Staining Solution (300µl for chamber slides) (ScienCell Research Laboratories, Inc., # 0223) was added to each well and the plates were incubated for 30 minutes at room temperature. Following incubation, the staining solution was carefully aspirated, and the cells were washed 5× with DI H_2O for 1 minute each to remove unbound and excess stain. Afterwards, the coverslips were mounted on glass slides using ProLong™ Diamond Antifade mounting medium (Invitrogen, # P36965) and the slides were dried, sealed with nail polish, and stored in the dark at 4°C until imaged.

3.4.2 Oil Red O Staining:

Adipogenic differentiation is generally associated with deposition of lipid or fat deposits in pre/mature adipocytes. To visualize such lipid or fat droplets in cells or tissue, Oil Red O staining is typically used (Kraus et al., 2016).

For Oil Red O staining, passage 4 BM-MSCs that were grown on glass coverslips, placed in 12-well plates for 2D culture system or 8-wells 3D chamber slides for 3D cell culture, were fixed with 4% paraformaldehyde in PBS, as mentioned above. After the fixative was removed, the cells were washed 3× with DI H_2O, and incubated with 1ml of working Oil Red O staining (300µl for 3D slides) solution per well for 25 minutes. Working Oil Red O solution is prepared from a stock solution (ScienCell Research Laboratories, Inc., # 0843) by diluting with DI H_2O in a 3:2 ratio and filtered using a 0.2µm syringe filter. After incubating for 25 minutes, the staining solution were removed, and the cells were washed 5× with DI H_2O. Afterwards, the coverslips were mounted on glass slides and stored at 4°C until imaged.

3.5 Immunohistochemistry:

Passage 4 BM-MSCs were grown and maintained on round coverslips, placed in 12-well 2D plates or 8-well 3D slides until confluency. For immunohistochemistry, growth/differentiation medium was gently removed from the plates and cells were washed once with PBS at room temperature for 1 minute. Afterwards, the cells were fixed with 1ml/well of 4% paraformaldehyde in PBS for the 12-well plate or 300µl/well for the 8-well 3D slides, for 15 minutes at room temperature. Then the fixative was carefully removed, and the plates were washed with PBS for 1 minute. Fixed cells were then permeabilized by

adding 1 ml of buffer (i.e., 0.5% Triton-X100 in PBS) per well and incubated for 5 minutes at room temperature. Afterwards, the permeabilization buffer was removed from the plates and the plates were washed twice with PBS for 1 minute. Permeabilized cells were then incubated with 250µl of 100nM Acti-stain™ 488 Phalloidin in PBS and were incubated for 30 minutes at room temperature in the dark. Following the phalloidin incubation, the phalloidin-PBS solution was removed from the plates and these were washed 3× with PBS for 1 minute. For counterstaining the nucleus/DNA, 300µl of DAPI (NucBlue® Fixed Cell ReadyProbes® Reagent) in PBS was added to each coverslip and incubated at room temperature for 5 minutes. Afterwards, the DAPI-PBS solution was removed from the plates and these were washed 3× with PBS for 1 minute. Following washing, the coverslips were carefully mounted on glass slides using Prolong Gold mounting medium. Afterwards, the coverslips were dried and sealed with nail polish, and stored in the dark at 4°C until imaged.

3.6 RNA Extraction, cDNA synthesis:

For gene expression analysis, RNA was isolated from confluent, passage four BM-MSCs grown in 12-well or 3D hydrogels in 24-well plates. Growth/differentiation medium was removed from each well and the cells were washed once with ice-cold PBS. Afterwards, the cells were then lysed by adding the appropriate amount of TRIzol™ Reagent (15596026). Trizol-lysed cell samples were homogenized, and the RNA, DNA, and proteins were separated in different layers by addition of chloroform and subsequent centrifugation at 12,000g for 15 minutes at 4°C. The RNA phase was carefully transferred into new 1.5ml centrifuge tube and then precipitated with isopropanol. The precipitated RNA was washed twice with 75% ethanol to remove any contaminant, and then dissolved

in RNAse-free water. RNA concentration and quality were analyzed using the NanoDrop 1000 spectrophotometer according to manufacturer's instruction and the integrity of RNA samples were analyzed using 8% agarose gel electrophoresis.

3.7 Gene Expression Analysis (qRT-PCR):

For gene expression analysis, single stranded cDNAs were prepared from 200ng of total RNA from all 2D and 3D cell samples using SuperScript® III First-Strand Synthesis SuperMix (Thermo Fisher Scientific, # 18080400) following manufacturer's protocol. Resultant cDNA samples were then diluted 5-fold to use in quantitative real time polymerase chain reaction (PCR) or qRT-PCR experiments, performed using Applied Biosystem's Step One plus instrument and Power SYBR™ Green PCR Master Mix (# 4367659), according to manufacturer's protocol. The primer sets for the analyzed genes are given below:

Table 1: List of primers for osteogenic and adipogenic transcription factors.

GAPDH	Forward primer	CAACGACCACTTTGTCAAGC
	Reverse primer	TTCCTCTTGTGCTCTTGCTG
RUNX2	Forward primer	GGAGTGGACGAGGCAAGAGTTT
	Reverse primer	AGCTTCTGTCTGTGCCTTCTGG
OSTERIX/SP7 (Osx)	Forward Primer	CCTCTGCGGGACTCAACAAC
	Reverse Primer	AGCCCATTAGTGCTTGTAAAGG
TWIST1	Forward primer	TTCTCGGTCTGGAGGATGGA
	Reverse primer	AATGACATCTAGGTCTCCGGC
PPARγ	Forward primer	CCTATTGACCCAGAAAGCGATT

	Reverse primer	CATTACGGAGAGATCCACGGA
C/EBPα	Forward primer	GCAAACTCACCGCTCCAATG
	Reverse primer	GGAAGGAGGCAGGAAACCTC
CHOP10/DDIT3	Forward Primer	GGAAACAGAGTGGTCATTCCC
	Reverse Primer	CTGCTTGAGCCGTTCATTCTC

3.8 Protein Extraction and Quantification:

3.8.1 Protein Extraction from BM-MSCs:

Total protein extracts from the cultured BM-MSCs were prepared using RIPA Lysis and Extraction Buffer (Thermo Fisher Scientific, # 89900) supplemented with Halt™ Protease and Phosphatase Inhibitor cocktail (100X) (Thermo Fisher Scientific, # 78442) with a final concentration of 1X. To extract total proteins, MSCs growth medium were aspirated from BM-MSCs cultured in 12-well plates or 24-well plates (3D culture), and the cells were washed twice with cold PBS (1ml/well in 12-well plate). After aspirating the PBS, 250µl of cold RIPA buffer containing the inhibitors were added to each well and the plates were placed on ice for 15 minutes, swirling every 3-5 minutes. After incubating in the ice, cells in the RIPA buffer were scraped from the plates using cell scrapers and the lysate was pipetted to homogenize the cells prior to transferring the lysates into 1.5ml centrifuge tubes. The cell lysates were further homogenized by rigorously vortexing for 1 minute. Afterwards, the protein lysate was sonicated for 1 minute to facilitate complete dissolution of cell wall and homogenization of the proteins. Sonicated cell extracts were then centrifuged at 14,000 g for 15 minutes at 4°C. After centrifugation, the protein

supernatants were transferred to fresh 1.5ml tubes and store at -80°C until used for protein quantification and SDS-PAGE/Western blot experiments.

3.8.2 Protein Quantification by Bradford Assay:

Protein samples were quantified using Bradford Protein assay, utilizing Coomassie Plus (Bradford) Assay Kit (Thermo Scientific, # 23236). Protein samples were thawed on ice and 50µl of protein samples were mixed with 1,500µl of Coomassie Plus reagent by inverting multiple times and incubating for 10 minutes at room temperature. Afterwards, the protein-Coomassie reagent mixture were transferred to disposable plastic cuvettes and their absorbance was measured at 595nm, using H_2O-Coomassie mixture as blank. The absorbances obtained from the samples were used to calculate corresponding protein concentration, using the standard equation obtained from the absorbance of bovine serum protein (BSA) dilutions (2,000µg/mL, 1,500µg/mL, 1,000µg/mL, 750µg/mL, 500µg/mL, 250µg/mL, 125µg/mL, and 25µg/mL).

Table 2: BSA dilutions and their absorbance for protein standard curve and Bradford quantification.

Standards	Absorbance	Absorbance (Avg.)	Concentration (ug/ml)
Sample 2000_1	1.509		
Sample 2000_2	1.657	1.555	2000
Sample 2000_3	1.499		
Sample 1500_1	1.388		
Sample 1500_2	1.358	1.356	1500
Sample 1500_3	1.321		
Sample 1000_1	1.216		
Sample 1000_2	1.154	1.166	1000
Sample 1000_3	1.129		
Sample 750_1	0.964		
Sample 750_2	0.951	0.954	750
Sample 750_3	0.947		
Sample 500_1	0.656		
Sample 500_2	0.663	0.673	500
Sample 500_3	0.701		
Sample 250_1	0.409		
Sample 250_2	0.368	0.368	250
Sample 250_3	0.327		
Sample 125_1	0.211		

Sample 125_2	0.172	0.191	125
Sample 125_3	0.189		
Sample 25_1	0.03		
Sample 25_2	0.047	0.036	25
Sample 25_3	0.03		

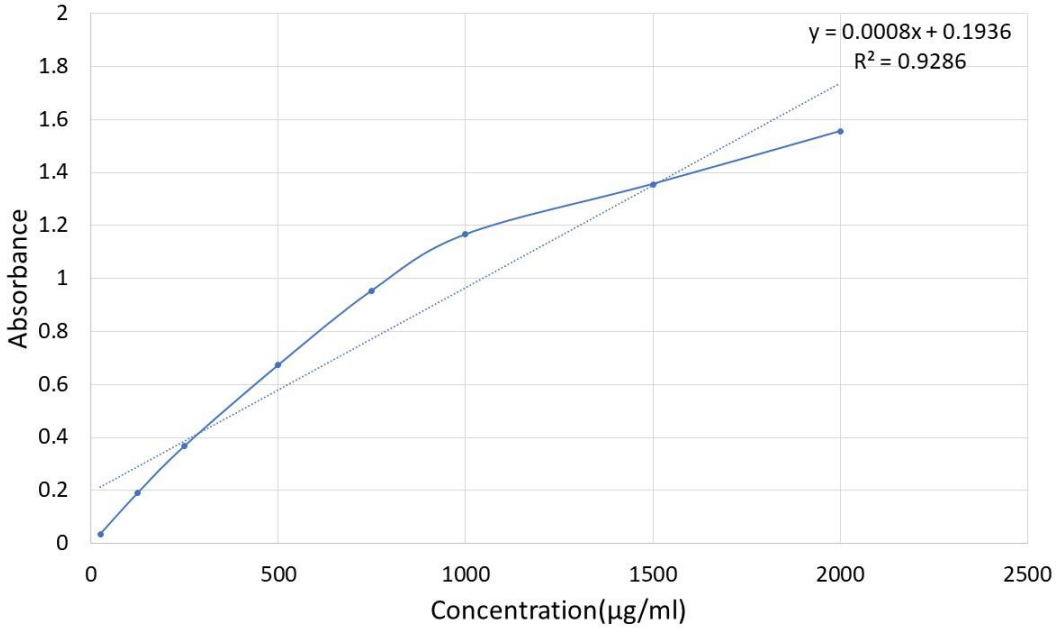

Figure 7: Protein standard curve generated from multiple dilution of bovine serum albumin (BSA) and their corresponding absorbance at 595nm. The equation from this curve is used quantify protein concentration of different samples.

3.9 SDS-PAGE Gel Electrophoresis and Western Blotting:

SDS-PAGE gel electrophoresis was used to separate the proteins based on their size. Thirty micrograms of total protein from all the protein samples were mixed in equal amounts of 2× protein loading buffer (Lammieli buffer) and were heated for 10 minutes at 65°C prior to loading into 10% Mini-PROTEAN® TGX™ Precast protein gels (Bio Rad, # 4561034). Gel tanks were filled with 1× running buffer (25mM Tris, 190mM Glycine, 0.1% SDS) and run for 1 hour at 110V. The proteins were transferred to a methanol-activated PVDF membrane using Bio Rad's fast transfer system. Following the transfer, the membranes were blocked with 5% BSA in TBST (TBS with 0.1% Tween 20) for 1 hour at room temperature. After blocking, the membranes were incubated with primary antibodies at 1:1,000 dilution, overnight at 4°C. Next day, the primary antibodies were removed, and the membranes were washed 3× with TBST for 10 minutes each, and then incubated with equal volumes of horseradish peroxidase (HRP)-tagged secondary antibodies in TBST at 1:2,000 dilution for 1 hour. After secondary antibody incubation, the membranes were washed 3× with TBST 10 minutes each and incubated for 5 minutes with Clarity™ Western ECL Substrate (# 1705060) before imaging.

All the membranes were stripped before incubating with primary antibodies. For stripping, imaged membranes were incubated in Restore™ Western Blot Stripping Buffer (Thermo Fisher Scientific, # 21059) for 15 minutes with rocking at room temperature. Stripped membranes were washed 3× for 10 minutes each and then blocked again, prior to incubating with next primary antibody.

Table 3: Concentration of primary and secondary antibodies for western blotting.

Antibody	**Dilution**
RUNX2 (Primary)	1:1000
PPARy (Primary)	1:1000
GAPDH (Primary)	1:1000
Anti-Goat HRP tagged Secondary Antibody	1:2000

3.10 Cell Viability/MTS Assay:

MTS cell proliferation/viability assay experiments were performed to evaluate cell viability of BM-MSCs encapsulated in PuraMatrix 3D hydrogel. Passage 4 BM-MSCs were encapsulated in 0.125% or 0.25% PuraMatrix with seeding density of 1×10^6 and 2×10^6 cells/ml in 96-well plates. Following encapsulation and adaptation of cells to the hydrogels, cells were treated with 20µl of CellTiter 96® AQ_{ueous} One Solution Reagent (Promega, # G3582) and incubated for 2.5 hours at 37°C in a humidified, 5% CO_2 atmosphere. Following incubation, the absorbance of the plates was measured at 490nm using a 96-well plate reader. MTS assays were done at Day 0, Day 3, and Day 7 of BM-MSC encapsulation.

Chapter 4: Characterization of BM-MSCs encapsulation in Corning® PuraMatrix™ Peptide Hydrogel.

4.1 Introduction:

Corning® PuraMatrix™ Peptide Hydrogel is a novel 3D culture system, consisting of 1% standard amino acids and 99% water. Unlike other polymer or hydrogel-based 3D culture system, PuraMatrix is completely synthetic, can be produced in large quantities, and is not known to elicit an immune response (Zhang et al., 1995). Largely, these features make PuraMatrix™ Peptide Hydrogel system an attractive tool for making cellular matrices for tissue engineering and regenerative medicine. To this end, multiple stem/progenitor cell types such as fetal human neural stem cells (hNSCs) (Thonhoff et al., 2008), rat liver progenitor cells (Semino et al., 2003), human microvascular endothelial cells (MVEC) (Narmoneva et al., 2005) and others have been tested for their ability to adapt and differentiate when encapsulated in PuraMatrix™ Peptide Hydrogel. However, BM-MSCs with PuraMatrix™ Peptide Hydrogel have not been characterized. Therefore, we sought to evaluate the ability of BM-MSCs to proliferate and differentiate when encapsulated in PuraMatrix™ Peptide Hydrogel.

4.2 Results:

4.1.1 BM-MSC viability in PuraMatrix™ Peptide Hydrogel with varying peptide concentration:

Stock PuraMatrix™ Peptide hydrogel consists of 1% (w/v%) peptide and 99% water, making it an 1% hydrogel system. Initially, we tested encapsulation of passage 4 BM-MSCs in 1%, 0.75%, 0.5%, 0.25%, and 0.125% peptide hydrogels; however, using bright field microscopy based morphological assessment, we found that BM-MSCs tend to be most adaptable to 0.125% and 0.25% peptide hydrogel, 0.125% hydrogel allowing them to reorganize themselves the most to interact with neighboring cells. Using MTS based cell viability assay, we have found that following post-encapsulation (immediately), viability of passage 4 BM-MSCs with a seeding density of 0.1×10^6cells/ml (2500 cells/well of a 96 well plate) in 0.125% peptide hydrogel is about 91% (91%±.03), compared to 2D cultured BM-MSCs (Figure 8). However, viability of BM-MSCs following encapsulation appears to be dependent on initial cell seeding density. With a seeding density of 0.2×10^6cells/ml (2500 cells/well of a 96 well plate), viability of BM-MSCs encapsulated in 0.125% PuraMatrix peptide hydrogel improves from 91% to 98% (98±.08) (Figure 8). Therefore, we propose that high seeding density is favorable for efficient encapsulation of BM-MSCs in PuraMatrix peptide hydrogel.

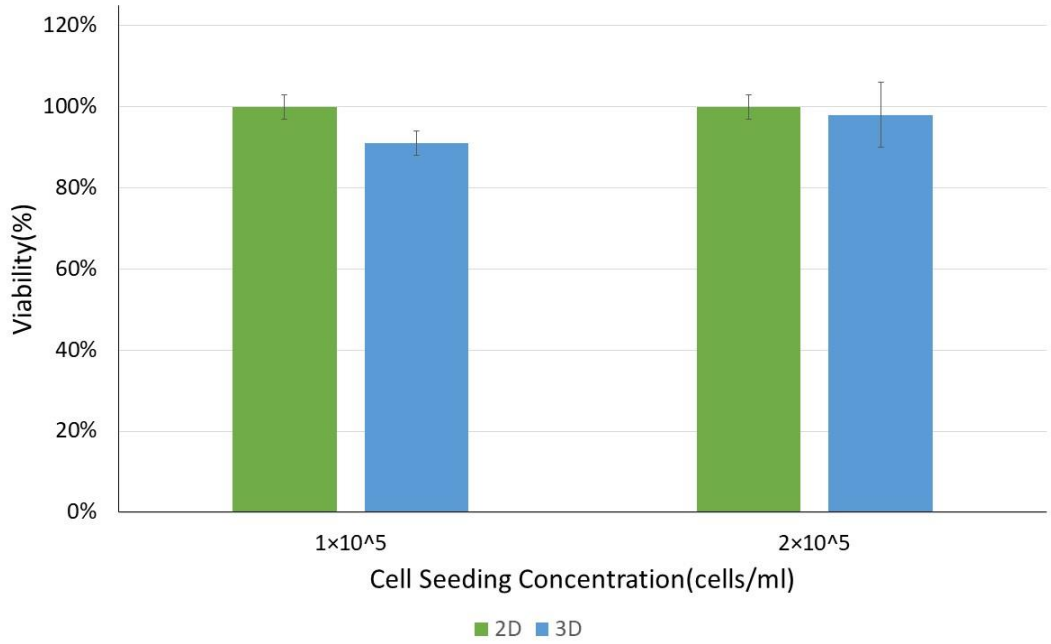

Figure 8: Viability of BM-MSCs encapsulated in 0.125% PuraMatrix peptide hydrogel.

4.1.2 Actin remodeling of BM-MSC encapsulated in Corning® PuraMatrix™ Peptide Hydrogel:

Although different cell types are characterized by their unique cellular shape and morphology, one key element of cellular architecture that plays a crucial role in determining cellular shapes and cellular motility is the actin filament. Actin and its accessory proteins are collectively referred as actin cytoskeleton. Due the cardinal function of actin cytoskeleton controlling cell shape and morphology, any cellular shape and/or morphologic assessment is usually determined by staining the actin with fluorescently labeled antibody or phalloidins conjugates and counterstaining the nucleus with DAPI.

Historically, MSCs or stromal cells have been considered to have fibroblast-like morphology which is represented by heir spindle shape. Part of this morphology and shape could also be attributed to the way MSCs have been cultured – as a monolayer in cell culture dishes. In the 2D cell culture plates/dishes, adherent MSCs attach to the plate surface and continue to proliferate/divide while being attached to the plate surface horizontally. Such attachment organizes the actin filaments in a flat elongated orientation known as stress fiber (Figure 10A). We reasoned that in a 3D microenvironment where cells can freely move within the matrix and can organize themselves, MSCs will adopt a different cellular organization and shape. As anticipated, undifferentiated passage 4 BM-MSCs encapsulated in 0.125% peptide hydrogel appeared to be round in shape and reorganize their actin cytoskeleton to interact with their neighbors and possess more lamellipodia and filopodia compared to their 2D grown counterparts (Actin staining was done 3 days post-encapsulation) (Figure 10B). We speculate that, in addition to new

structural organization, hydrogel-encapsulated BM-MSCs may behave and express cytokines/chemokines differently.

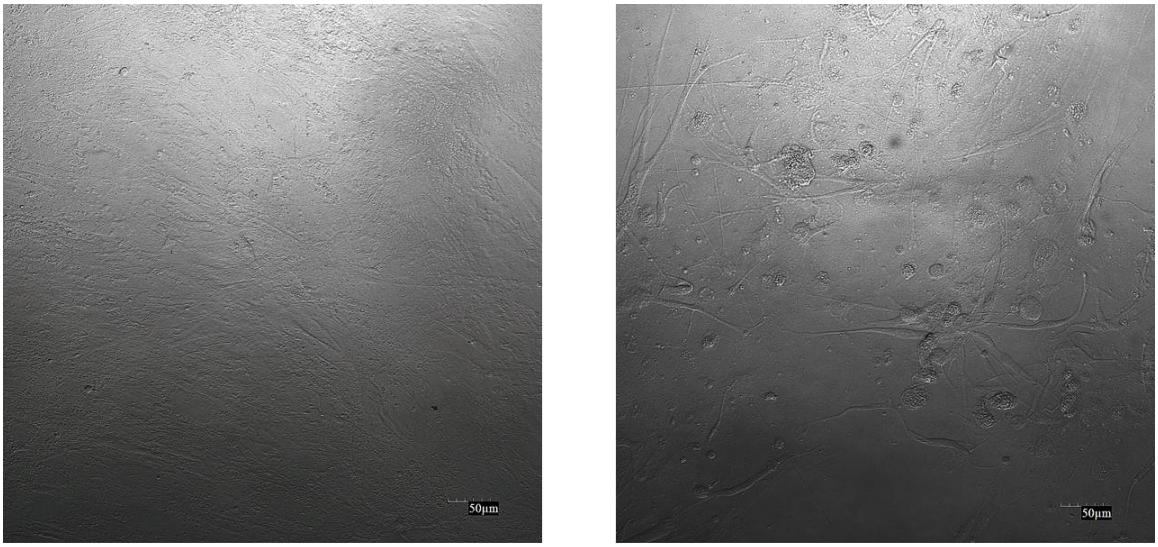

Figure 9: Bright-field microscopy analysis of passage 4 BM-MSCs cultured in (A) 2D culture plated and (B) encapsulated in 3D PuraMatrix peptide hydrogel (Scale bar = 50µm).

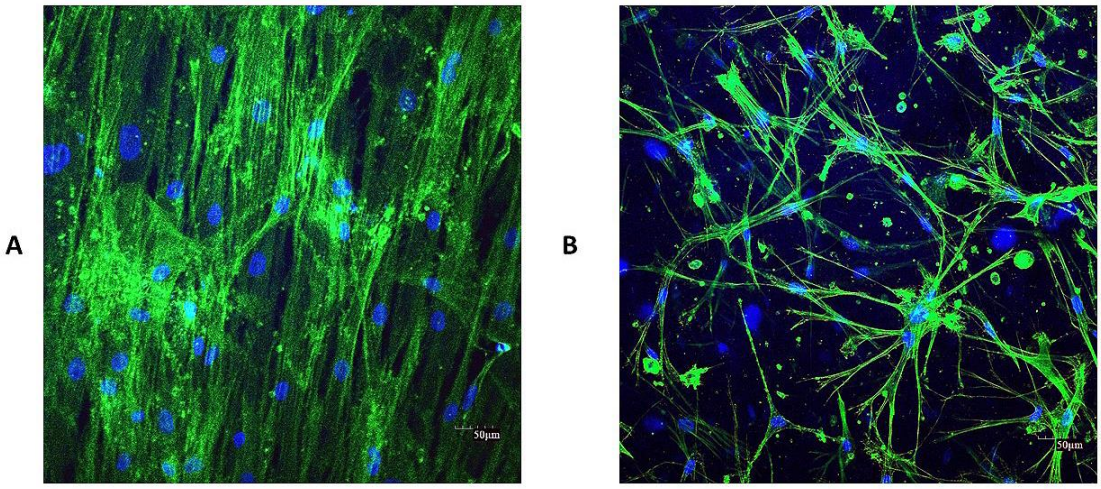

Figure 10: Morphological analysis of (A) 2D and (B) 3D culture BM-MSCs (B) using immunohistochemistry. Actin filament (green) and nucleus (blue) of BM-MSCs were stained using alexa fluor 488 phalloidin and DAPI respectively, showing the differential actin organization of BM-MSCs in 2D and 3D culture system. In 2D culture system, BM-MSCs (Scale bar = 50µm).

Chapter 5: Transcriptional analysis of key osteogenic and adipogenic transcription factor during BM-MSC differentiation in 2D and 3D culture systems.

5.1 Gene expression analysis osteogenic differentiation of BM-MSCs in 2D and 3D culture:

5.1.1 Introduction:

Multipotency of BM-MSCs enables them to differentiate into mesodermal lineages such as osteogenic, adipogenic, and chondrogenic lineages. We were particularly interested in osteogenesis and adipogenesis of BM-MSCs because commitment to these lineages is reciprocally regulated by BM-MSCs throughout animal development and in certain disease conditions. Upon exposure to osteogenic stimuli (hormones, growth factors, etc.), BM-MSCs start to specialize into pre-osteoblast progenitor cells and this commitment restricts their differentiation to adipogenic or chondrogenic lineages (Javed et al., 2010; Fakhry et al., 2013). Pre-osteoblast cells differentiate into immature osteoblast as a result of elevated expression of Runx2, Osx, and Dlx5. The transition of immature to mature osteoblast, however, is inhibited by Runx2 (Komori, 2006; Karsenty et al., 2009). At this time point, other osteogenic transcription factors such as Msx, and Dlx3 play key roles and allow immature osteoblast to become mature osteoblast. We sought to explore how Runx2, Osx, and Twist expression is differentially modulated during the course of osteogenic

differentiation, at different time point. We also wanted to evaluate if growth in a 3D microenvironment affects expression pattern of these transcription factors.

5.1.2 Results:

At first, we sought to evaluate if maintenance of undifferentiated hBM-MSCs in PuraMatrix based 3D hydrogel, in contrast to 2D culture, have any effect on GAPDH as well as osteogenic (RUNX2, OSX, and TWIST1) and adipogenic transcription factors (PPARγ, C/EBPα, and CHOP10).

We have found that besides OSX and C/EBPα, expression of GAPDH, RUNX2, TWIST1, PPARγ, and CHOP10 significantly ($p < 0.00001$) decreases when hBM-MSCs are encapsulated in 0.125% PuraMatrix peptide hydrogel (Figure 11). On average, in 3D culture GAPDH expression could be detected after 5 cycle (5.3±0.15) ($p < 0.00001$) over 2D, RUNX2 about 4 cycle (4.05±0.44) ($p < 0.00001$), TWIST1 about 6 cycle (5.73±0.30) ($p < 0.00001$), PPARγ about 2 cycle (1.94±0.14) ($p < 0.00001$), and CHOP10 about 6 cycle (6.35±0.34) ($p < 0.00001$).

To analyze the relative expression of RUNX2, OSX, and TWIST1 during osteogenic differentiation of BM-MSCs, we collected total RNAs from 2D and 3D cultured cell samples at Day 0 (undifferentiated control), Day 3, Day 7, Day 14, and Day 21 of differentiation. cDNA made from the total RNA samples were used in performing quantitative PCR (qPCR) for analyzing gene expression. Gene expression data sets were analyzed and fold change were calculated using delta delta CT method (Livak and Schmittgen, 2001). Expression data were normalized to GAPDH expression.

Compared to the control undifferentiated BM-MSCs (Day 0), *RUNX2* expression increased significantly about 1.8 fold (1.81±.5) ($p = 0.04$) at Day 3, about 1.86 fold (1.86±0.54) ($p= 0.05$) at Day 7, about 2.03 fold (2.03±0.56) ($p = 0.04$) fold at Day 14, and about 3.6 fold (3.61± 0.41) ($p = 0.003$) fold at Day 21 of osteogenic differentiation, in 2D culture system (Figure 12). Considering Runx2 expression is expected to increase over the course of differentiation, particularly when MSC commits to pre-osteoblast progenitors and forms immature-osteoblast, our *RUNX2* expression profile is consistent with established tenet.

In contrast to 2D system, *RUNX2* expression did not significantly increase (1.09±0.60) ($p = 0.74$) at Day 3 relative to Day 0 (undifferentiated control) or change (.90±0.48) ($p = 0.62$) over control at Day 7 suggesting basal level of expression up to Day 7 of differentiation. However, RUNX2 expression significantly increased, about 3.4 fold (3.38±0.46) ($p = 0.004$) over control at Day 14, and 8.9 (8.94±0.95) ($p = 0.01$) fold increment at Day 21 of osteogenic differentiation in 3D culture (Figure 12). Although RUNX2 expression in 3D culture system follow same pattern of expression as the 2D culture system and the expression profile reported by other studies, any fold change difference between 2D and 3D culture system, at different time point during differentiation may largely be due to the difference in metabolic and morphological changes associated with BM-MSCs adapting to a 3D microenvironment.

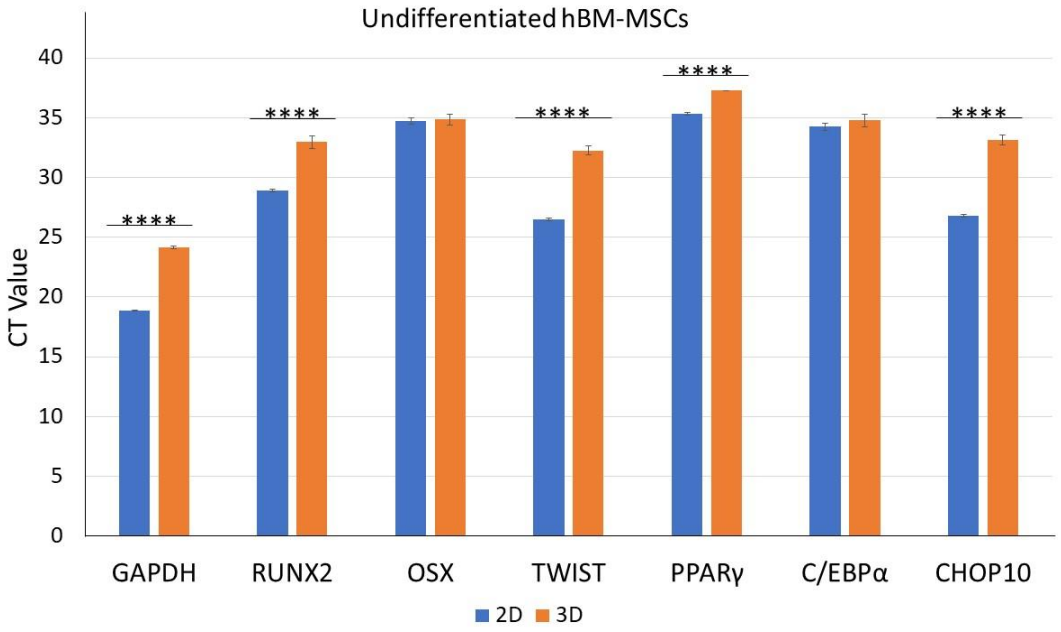

Figure 11: Differential expression of GAPDH, RUNX2, OSX, TWIST, PPARγ, C/EBPα, and CHOP10 transcription factors between undifferentiated hBM-MSCs from 2D and 3D PuraMatrix hydrogel.

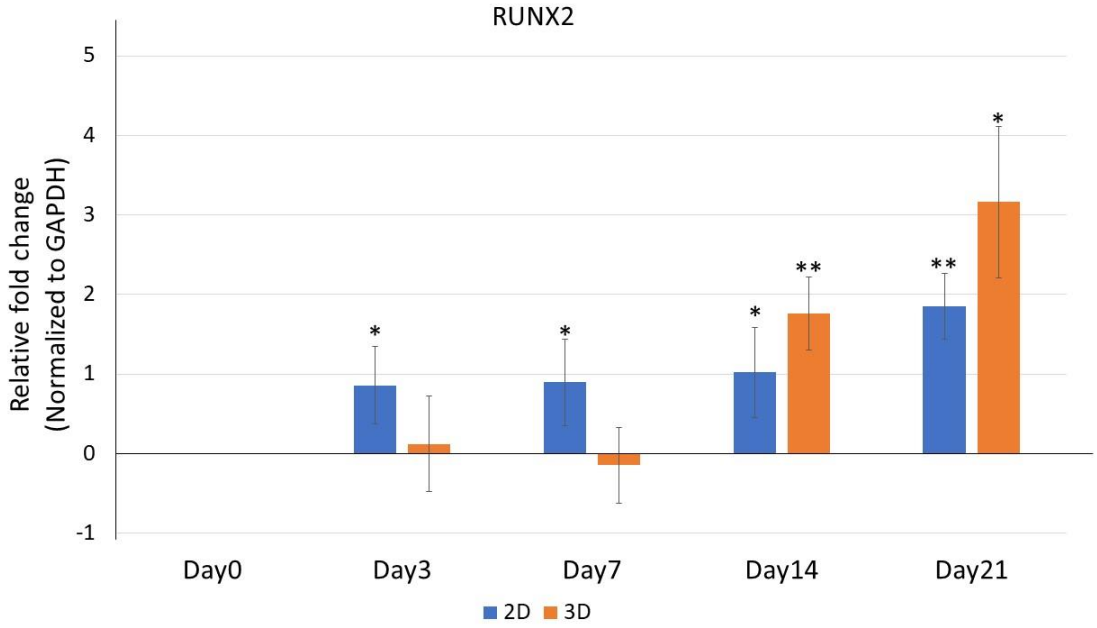

Figure 12: Differential expression of *RUNX2* during osteogenic differentiation of BM-MSCs in 2D and PuraMatrix based 3D culture. qPCR analysis shows the relative change in *RUNX2* expression (relative to undifferentiated hBM-MSCs) at Day 3, Day 7, Day 14, and Day 21 of differentiation, normalized to GAPDH. n = 3 and error bars = standard error of the mean. "*" means $p < 0.05$, "**" means $p < 0.01$, "***" means $p < 0.001$, and "****" means $p<0.0001$.

For Osterix (*OSX*), *OSX* expression significantly increased about 13.3 fold (13.27± 0.67) (p = 0.01) at Day 3 of osteogenic differentiation in 2D culture system, compared to undifferentiated control (Day 0) BM-MSCs (Figure 13). However, *OSX's* expression decreased about ~12 fold down to basal level (1.14± 0.21) (p = 0.3) at Day 7 and continued to be expressed slightly elevated or basal level, over control, at Day 14 (1.55 ± 0.72) (p = 0.3) and Day 21 of osteogenic differentiation (1.58± 0.47) (p = 0.13) in 2D culture system (Figure 13). This observation suggests that OSX is an early osteogenic regulator, functioning at the early stage of differentiation.

Interestingly, in 3D culture system, *OSX* expression significantly decreased about 5-fold (0.18± 0.69) (p = 0.02) at Day 3 of osteogenic differentiation in 2D culture system, compared to control (Day 0, undifferentiated) BM-MSCs and continued to decrease about 20-fold (.05± 0.47) (p = 0.0007) over control at Day 7 (Figure 13). *OSX* started to increase after Day 7, and at Day 14, OSX expression increased about 2.8 fold (2.77 ± 0.88) (p = 0.09) and about 5.4 fold (5.43± 0.52) (p = 0.006) over control at Day 21 of osteogenic differentiation (Figure 13).

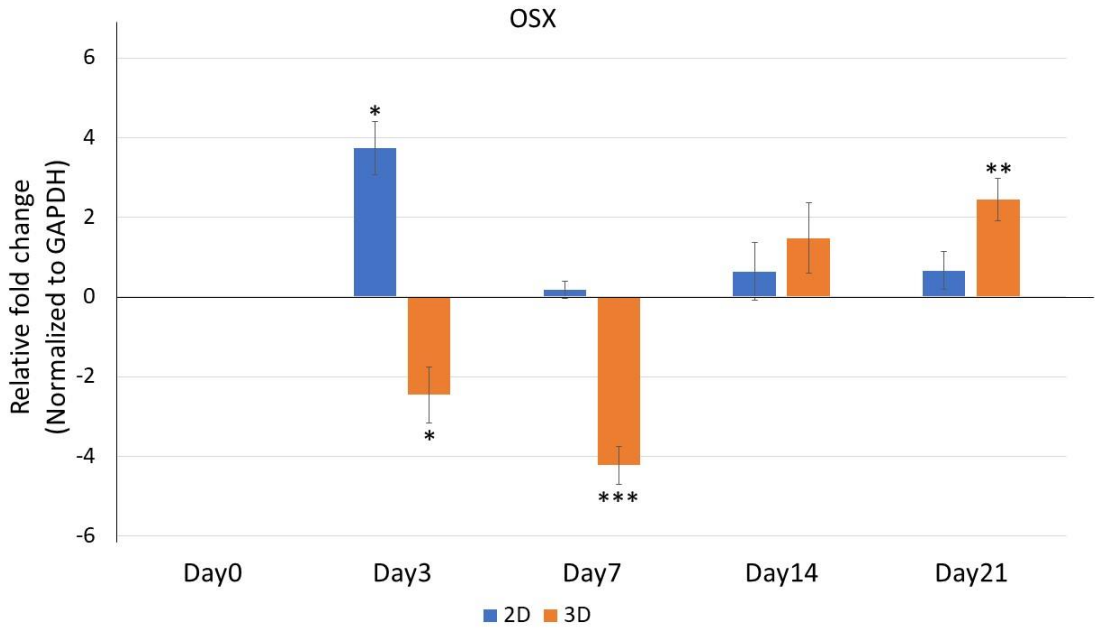

Figure 13: Differential expression of *OSX* during osteogenic differentiation of BM-MSCs in 2D and PuraMatrix based 3D culture. qPCR analysis shows relative change in *OSX* expression (relative to undifferentiated hBM-MSCs) at Day 3, Day 7, Day 14, and Day 21 of differentiation, normalized to GAPDH. n = 3 and error bars = standard error of the mean. "*" means $p < 0.05$, "**" means $p < 0.01$, "***" means $p < 0.001$, and "****" means $p<0.0001$.

Considering TWIST1 is a negative regulator of MSCs osteogenesis, we expected to see reduction of *TWIST1* at the early stage of differentiation and continued repression or basal level expression during the differentiation of BM-MSCs into mature osteoblasts.

In 2D culture system, *TWIST1* expression significantly increased about 9.1 fold (9.09 ± 0.94) ($p = 0.01$) at Day 3 of osteogenic differentiation in 2D culture system, compared to Day 0 BM-MSCs (undifferentiated control) (Figure 14). However, at Day 7 *TWIST1* expression decreased about ~2 fold to 7.9 fold (7.90± 0.58) ($p = 0.001$) over control and was only trending to be lower than control at Day 14 (0.67 ± 0.61) ($p = 0.19$) and about the same over control at Day 21 (0.93±0.48) fold ($p = 0.74$) of osteogenic differentiation, in 2D culture system (Figure 14).

Surprisingly, in 3D culture system, *TWIST* expression had a trend towards decreased expression over control (about 1.6 fold) (0.64± 1.03) ($p = 0.3$) at Day3 of osteogenic differentiation in 2D culture and continued to trend towards a decrease of 2.2 fold (.46± 0.10) ($p = 0.2$) over control at Day 7. Interestingly, *TWIST* started to increase after Day 7, and at Day 14, *TWIST* expression increased about 1.7 fold (1.71± 1.12) ($p = 0.31$) over control, and about 1.9 fold (1.89± 1.03) ($p = 0.2$) at Day 21 of osteogenic differentiation (Figure 14). Considering TWIST did not change significantly during the course of osteogenic differentiation in 3D culture system, it is possible that TWIST is expressed at basal level and does not undergo significant down regulation in 3D culture system.

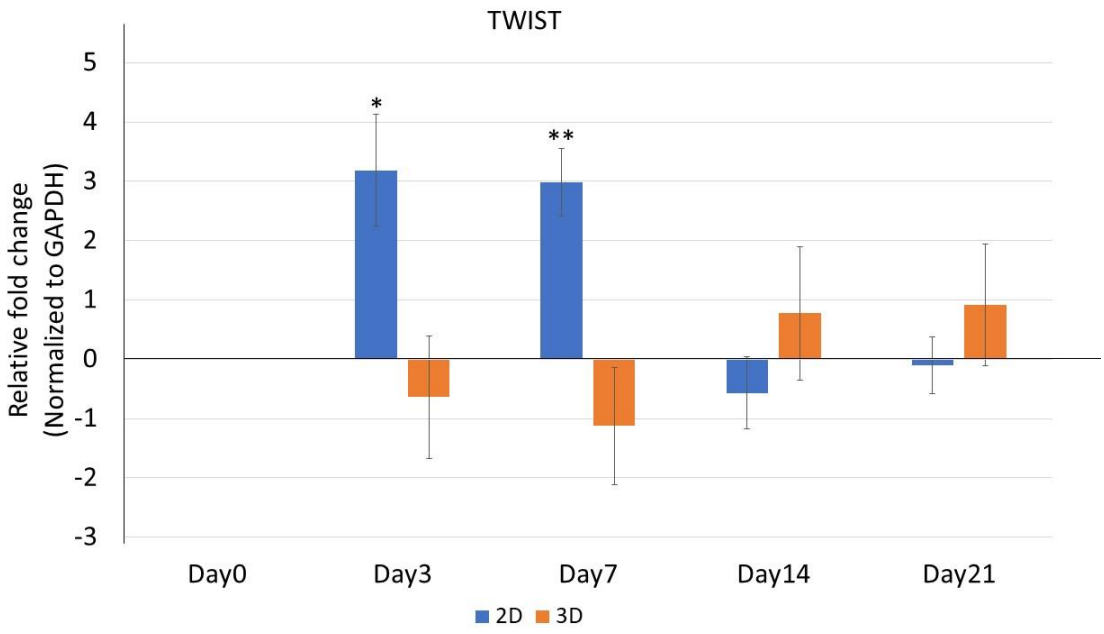

Figure 14: Differential expression of *TWIST* during osteogenic differentiation of BM-MSCs in 2D and PuraMatrix based 3D culture. qPCR analysis shows relative change in *TWIST* expression (relative to undifferentiated hBM-MSCs) at Day 3, Day 7, Day 14, and Day 21 of differentiation, normalized to GAPDH. n = 3 and error bars = standard error of the mean. "*" means $p < 0.05$, "**" means $p < 0.01$, "***" means $p < 0.001$, and "****" means $p<0.0001$.

5.2 Gene expression analysis of adipogenic differentiation of BM-MSCs in 2D and 3D culture:

5.2.1 Introduction:

Adipogenesis of MSCs or adipo-progenitor cells begins with commitment towards adipogenic lineage in response to adipogenic stimuli (hormones, growth factors, etc.). Adipogenic stimuli activate a series of signal transduction cascades that lead to high level expression of ERG2, and CREB, and expression of these early adipogenic activators initiates adipogenic commitment in MSCs or adipogenic progenitors (Karsenty et al., 2009; Javed et al., 2010). Following commitment, terminal differentiation takes place once C/EBPβ is activated and expressed at high level followed by C/EBPγ expression at the early stage of terminal differentiation. Activated C/EBPβ then activates C/EBPα, which then activates PPARγ. PPARγ and C/EBPα have an inbuilt auto regulatory feedback system where activated PPARγ autoactivates itself as well as C/EBPα (Javed et al., 2010; Fakhry et al., 2013; Bruderer et al., 2014). C/EBPα also continues to promote PPARγ expression until the pro-adipocytes differentiate into mature adipocytes. In addition to terminally differentiating into mature adipocytes, both PPARγ and C/EBPα play key role in maintaining mature adipocyte identity (Fakhry et al., 2013; Bruderer et al., 2014).

To analyze gene expression pattern of *PPARγ*, *C/EBPα*, and *CHOP10* during adipogenesis of BM-MSCs, total RNAs from cell samples at Day 0 (undifferentiated control), Day 3, Day 7, Day 14, and Day 21 of differentiation was isolated, and cDNA was made to perform quantitative PCR (qPCR). Gene expression analysis was performed using delta delta CT method (Livak and Schmittgen, 2001). Expression data were normalized to GAPDH expression.

5.2.2 Results:

Compared to control (Day 0, undifferentiated) BM-MSCs, *PPARγ* expression significantly increased, about 9.9 fold (9.85± 0.93) (p = 0.02) at Day 3 but decreased to about 5.7 fold (5.72± 0.44) (p = 0.002) over control at Day 7. However, *PPARγ* expression again increased about 11.1 fold (11.11± 1.25) (p = 0.04) fold at Day 14, and about 29 fold (28.85±0.55) (p = 0.0009) at Day 21 of adipogenic differentiation, over control, in 2D culture (Figure 15).

Interestingly, in 3D culture system, *PPARγ* expression increased about 41 fold (40.82± 1.70) (P = 0.03) over control at Day 3, but markedly downregulated to basal/control level (0.96 ± 2.36) (p = 0.965456918) at Day 7 of adipogenic differentiation (Figure 15). However, *PPARγ* expression again trended toward an increase of about 5.6 fold (5.56 ± 2.72) (p = 0.3) at Day 14, and about 8 fold (7.98 ± 1.56) (p = 0.07) over control at Day 21 of differentiation, in 3D culture (Figure 15). Although expression pattern of *PPARγ* in 3D culture correlates with that of in 2D culture, the relative difference in the fold change is due to different unique gene expression program active in 3D culture BM-MSCs upon encapsulation.

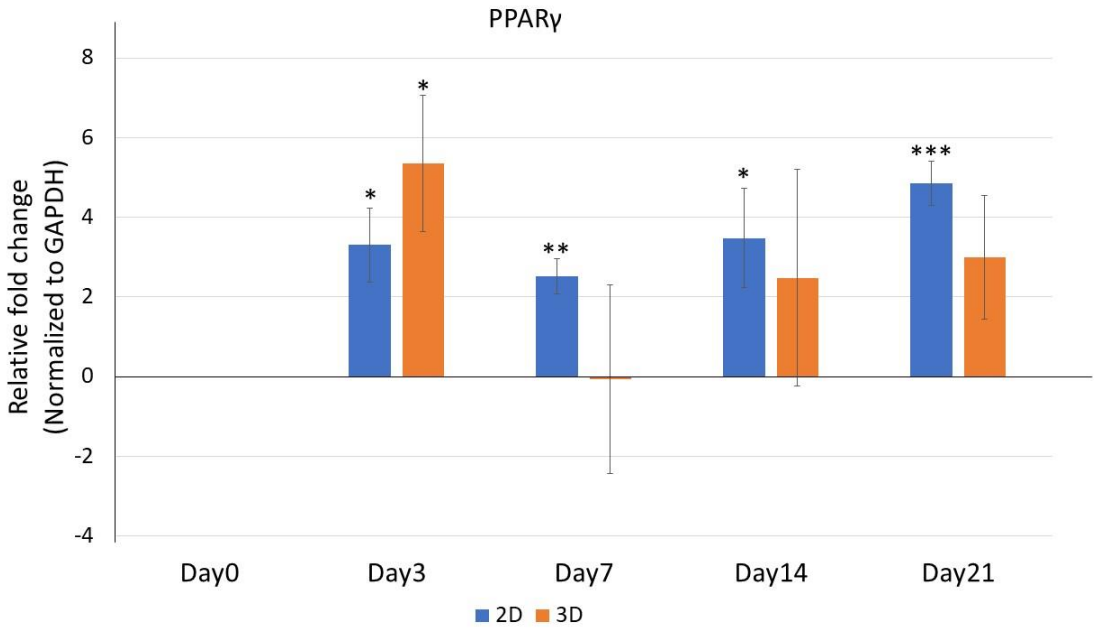

Figure 15: Differential expression of *PPARγ* during adipogenic differentiation of BM-MSCs in 2D and PuraMatrix based 3D culture system. qPCR analysis shows relative change in *PPARγ* expression (relative to undifferentiated hBM-MSCs) at Day 3, Day 7, Day 14, and Day 21 of differentiation, normalized to GAPDH. n = 3 and error bars = standard error of the mean. "*" means $p < 0.05$, "**" means $p < 0.01$, "***" means $p < 0.001$, and "****" means $p < 0.0001$.

Expression of *C/EBPα* increased significantly, about 897 fold (897.44± 1.16) (p = 0.0002) at Day 3 of adipogenic differentiation, compared to control (Day 0, undifferentiated) in 2D culture (Figure 16). However, *C/EBPα* expression decreased to about 9 fold increment over control (8.93± 1.08) (p = 0.01) at Day 7 of differentiation and then decreased to 6.1 fold over control (6.09±1.04) (p = 0.02) at Day 14 of differentiation. However, *C/EBPα* expression again significantly upregulated, about 21 fold over control (21.01±0.94) (p = 0.009) at Day 21 of differentiation (Figure 16).

Unexpectedly, in 3D culture system, *C/EBPα* expression significantly decreased about 6.6 fold over control (0.15±1.71) (p = 0.05) at Day 3 of differentiation but returned to basal level (1.24±3.36) (p = 0.9) over control at Day 7 of differentiation (Figure 16). However, *C/EBPα* expression continued to be expressed at basal level (.60±2.87) (p = 0.7) at Day 14 and Day 21 (0.76±2.86) (p = 0.7) of differentiation. Considering C/EBPα is a direct transcriptional target of PPARγ (with an inbuilt auto-regulatory feedback system that promotes both of these transcription factors expression), low PPARγ expression between Day 3 and Day 14 of adipogenic differentiation in 3D culture might lead to basal level expression of C/EBPα at that time period.

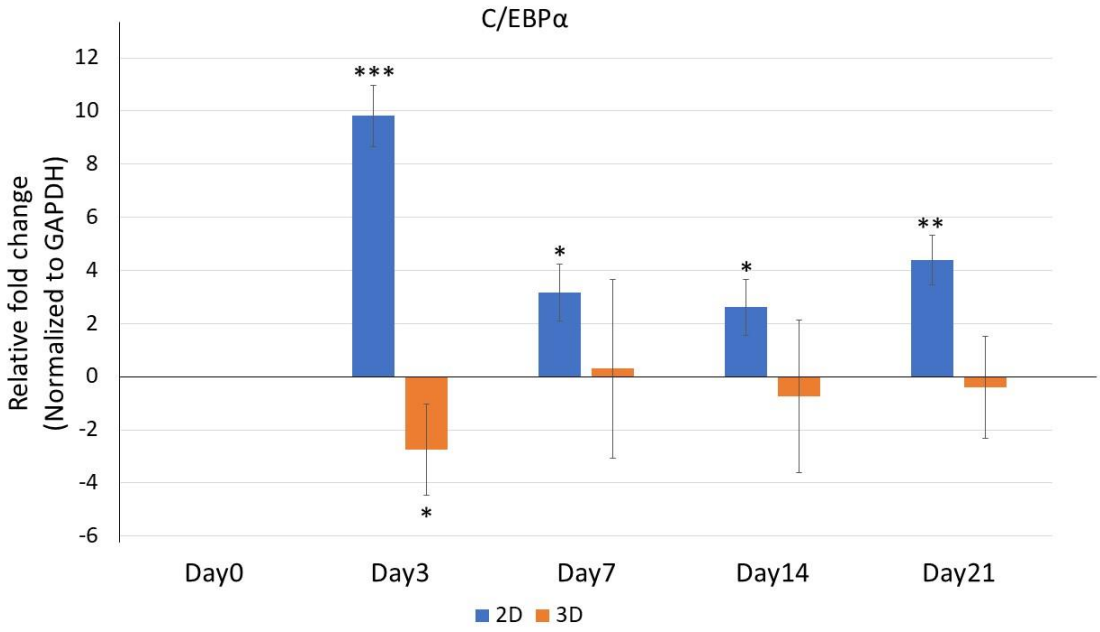

Figure 16: Differential expression of *C/EBPα* during adipogenic differentiation of BM-MSCs in 2D and PuraMatrix based 3D culture system. qPCR analysis shows relative change in *C/EBPα* expression (relative to undifferentiated hBM-MSCs) at Day 3, Day 7, Day 14, and Day 21 of differentiation, normalized to GAPDH. n = 3 and error bars = standard error of the mean. "*" means $p< 0.05$, "**" means $p< 0.01$, "***" means $p< 0.001$, and "****" means $p<0.0001$.

CHOP10 is a negative regulator of adipogenesis and have been found to be expressed at elevated level at undifferentiated MSCs and early stage of differentiation in and pre-adipocyte cell lines. Therefore, we expected to see suppression of *CHOP10* expression following differentiation.

In 2D culture system, *CHOP10* expression significantly downregulated about 3 fold (0.33±0.68) ($p = 0.03$) at Day 3, and about 2.6 fold (0.39±.92) ($p = 0.09$) at Day 7 of differentiation, over control (Day 0, undifferentiated BM-MSCs) (Figure 17). *CHOP10* expression continued to decrease about 4.8 fold over control (0.21±0.62) ($p = 0.005$) at Day 14 and about 2.3 fold (0.43±0.58) ($p = 0.03$) at Day 21 of differentiation (Figure 17).

Surprisingly, in 3D culture system, *CHOP10* expression did not change (1.23 ±3.01) ($p = 0.9$) at Day 3 (control undifferentiated BM-MSCs) or at Day 7 (.98±2.86) ($p = 0.9$) of differentiation, over control (Figure 17). Instead, *CHOP10* continued to be expressed at basal level at Day 14, (1.24±2.84) ($p = 0.9$) and Day 21 of differentiation (1.02±1.04) ($p = 0.9$) (Figure 17).

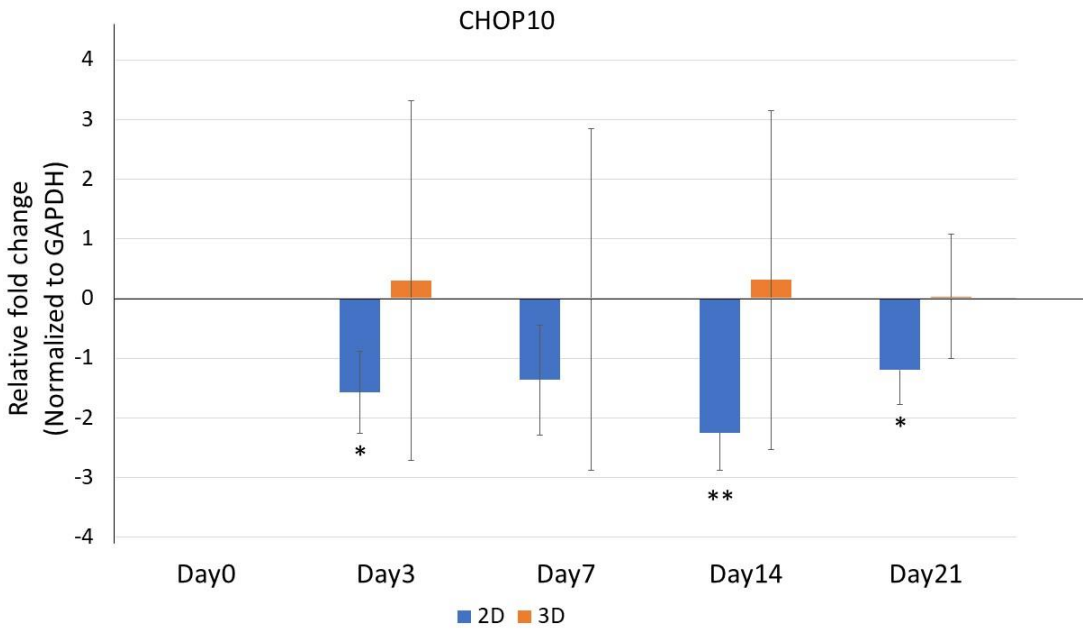

Figure 17: Differential expression of *CHOP10* during adipogenic differentiation of BM-MSCs in 2D and PuraMatrix based 3D culture. qPCR analysis shows relative change in *CHOP10* expression (relative to undifferentiated hBM-MSCs) at Day 3, Day 7, Day 14, and Day 21 of differentiation, normalized to GAPDH. n = 3 and error bars = standard error of the mean. "*" means $p < 0.05$, "**" means $p < 0.01$, "***" means $p < 0.001$, and "****" means $p<0.0001$.

Chapter 6: Translational analysis of master osteogenic and adipogenic transcription factor during BM-MSCs differentiation in 2D and 3D culture system.

6.1 Introduction:

RUNX2 and PPARy are considered the master regulator of osteogenesis and adipogenesis, respectively. Previous studious suggests that, ectopic expression of these transcription factors is sufficient to induce osteogenic and adipogenic differentiation in MSCs or any other cell types and their depletion drastically affect skeleton development and fat metabolism. Since we found dynamic transcript level expression of *RUNX2* and *PPARy* at different stage of differentiation, we sought to evaluate if their protein level expression correlate with their transcript level expression.

With equal amount of total protein from all the 2D and 3D protein extracts, we performed SDS-PAGE and transferred the separated protein to a PVDF membrane for Western blotting. Following incubation with RUNX2, PPARy, and GAPDH antibodies, we have found that compared to control (Day 0, undifferentiated) samples, there is slight increase of RUNX2 protein expression at Day 3 of osteogenic differentiation in 2D culture system, with marked elevation of RUNX2 protein at Day 7 of osteogenic differentiation (Figure 18). Such protein level expression of RUNX2 is consistent with its transcript level change during osteogenesis; although, relative change of protein level between Day 3 and Day 7 of differentiation is much stronger than its transcript level difference. Surprisingly,

we did not find any RUNX2 protein in our 3D culture extracts from osteogenic differentiation, at Day 0, Day 3, and Day 7 despite high level of total protein content found in the corresponding 3D protein extracts (Figure 18). We speculate that residual RAD16 oligopeptide from the PuraMatrix hydrogel might interfere with RUNX2 antibody binding to corresponding RUNX2 proteins in the membrane. Such interaction might be highly selective between RAD16 and RUNX2 antibodies considering PPARy and GAPDH antibodies did work for our 3D western blot experiments. It would be useful to analyze RUNX2 protein expression in 3D osteogenic differentiation samples using RUNX2 antibodies from different vendors or host animal.

Figure 18: Western blot analysis of RUNX2's protein level expression between 2D and 3D cultured BM-MSCs at Day 0 (control), Day 3 and Day 7 of osteogenic differentiation. GAPDH is used as loading control.

In the case of PPARγ, its expression at protein level was markedly increased at Day 3 of adipogenic differentiation of BM-MSCs in 2D culture system; however, we did not find any noticeable expression at Day 7 of differentiation (Figure 19). Interestingly, in 3D culture system we found noticeably high expression of PPARy at Day 7 of differentiation compared to control. However, we did not find any expression of PPARy at Day 3 of adipogenic differentiation in the 2D culture system (Figure 19). As we expected, GAPDH was expressed at a similar level throughout the osteogenic and adipogenic differentiation, in both 2D and 3D culture system (Figures 18,19).

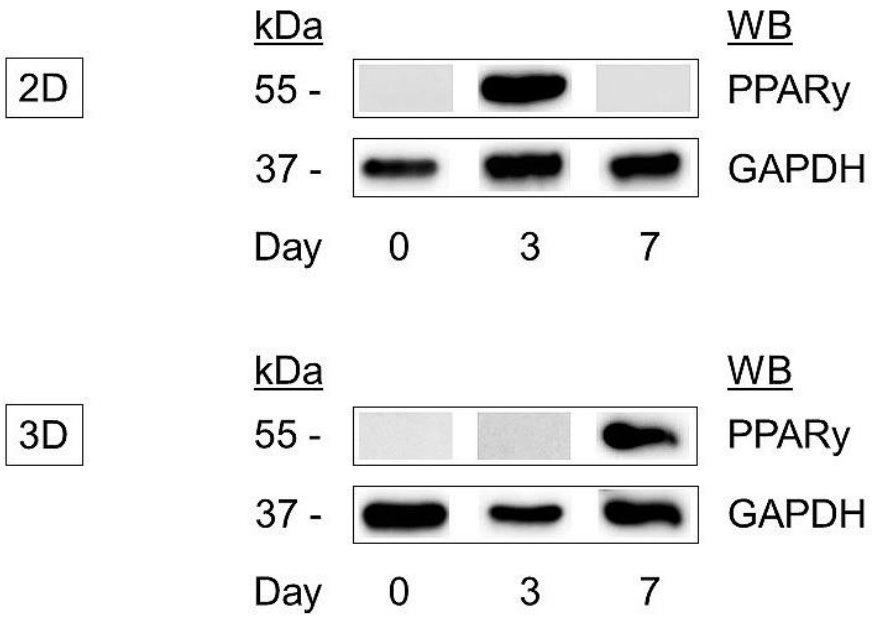

Figure 19: Western blotting analysis of PPARγ's protein level expression between 2D and 3D cultured BM-MSCs at Day 0 (control), Day 3 and Day 7 of adipogenic differentiation. GAPDH is used as loading control.

Chapter 7: Discussion and Conclusion.

Discussion:

Osteogenesis in MSCs *in vitro* is initiated by supplementing MSCs growth medium with osteo-inductive supplements such as Dexamethasone, L-ascorbate and β glycerol-3-phosphate (Pittenger, 2008; Castren et al., 2015). Together, these supplements activate a series of signaling cascades of which BMP and WNT signaling pathway is of significant importance with regards to instigating osteogenic commitment in MSCs (Figure.3). Wnt-B-catenin pathway not only inhibits pro-adipogenic transcription factor C/EBPα and PPARγ – the master adipogenic transcription factor, it also activates Runx2 - the master osteogenic transcription factor - as well as Dlx5 - another key osteogenic transcription factor (Kang et al., 2007). BMP-Smad signaling on the other hand directly activates Runx2 and promotes osteogenesis whilst restricting myogenic differentiation (Lee et al., 2000). Activated Runx2 then differentiates MSCs or pre-osteoblast progenitors to pre-osteoblast and immature osteoblast (Komori, 2010; Fakhry et al., 2013). OSX is upregulated during MSCs-to-preosteoblast transition and in association with RUNX2, OSX promotes preosteoblast-to-immature osteoblast transition. Differentiation of immature osteoblast to mature osteoblast requires activation of factors associated with extracellular matrix protein production and matrix maturation such as Fra1 and Atf4 hBM-MSCs (Komori, 2006).

In osteogenic differentiation experiments in 2D culture system, we found that compared to undifferentiated hBM-MSCs, expression of *RUNX2* increases significantly about 1.6 fold, 1.9 fold, 2.02 fold, and 3.6 fold at Day 3, Day 7, Day 14, and Day 21 of osteogenic differentiation, respectively (Figure 12). However, in a previous study with murine MC3T3-E1 preosteoblast cell line, Xiao et al., (1998) showed that *Runx2* increases about 1.3-fold, 1.5 fold, 2.1 fold, 2.8 fold, and 3.0 fold at Day 0.5, Day 1, Day 2, Day 4, and Day 6 of osteogenesis, respectively (Xiao et al., 1998). Although *RUNX2* expression pattern (upregulation) during osteogenesis in murine preosteoblast cell line correlates with that of in hBM-MSCs cells, the relative expression level of *RUNX2* at different time points, however, do vary between these two cell types. One plausible rationale behind such variation might be the difference in developmental progression between MSCs and pre-osteoblast cells. Pre-osteoblast cells are already committed to osteogenic differentiation and expected to express *Runx2* already whilst BM-MSCs or MSCs need to commit to osteogenic lineage in response to osteogenic stimuli and then convert to preosteoblasts. The developmental timing and epigenetic/transcriptional changes required for such progression might explain relative difference in *RUNX2* transcript level at different time point during osteogenesis, between different cell types.

In our 3D culture system, *RUNX2*, however, continued to be expressed at a basal level until Day 7 of differentiation (Figure 12). Interestingly, at Day 14, *RUNX2* expression significantly increases about 3.4 fold and continues to increase with an 8.9 fold increment over control at Day 21 of differentiation (Figure 12). Although the upregulated expression pattern of *RUNX2* in 3D culture system is similar to that of 2D culture system, we have found significant upregulation of *RUNX2* at Day 14 and Day 21 of osteogenesis in 3D

culture system. Marked upregulation of *RUNX2* at the late stage of osteogenic differentiation in 3D culture system suggests improved osteogenesis. Considering the differentiation process itself is very inefficient - only a portion of the entire stem cell population terminally differentiates, it is possible that during osteogenic differentiation of hBM-MSCs in 3D peptide hydrogel system, only a small fraction of encapsulated hBM-MSCs enters differentiation at Day 3 or Day 7 while a large number of undifferentiated hBM-MSCs progress towards osteogenesis at between Day 14 and Day 21.

As anticipated, RUNX2's protein level expression does correlate with its transcript level expression in 2D culture system. Our western blotting experiments have found that compared to control (Day 0), RUNX2 protein level slightly increases at Day 3 of differentiation whereas a marked elevation of RUNX2 protein was found at Day 7 of osteogenic differentiation in 2D culture system (Figure 18). Surprisingly, we did not find any RUNX2 protein in our Day 3, Day 7 samples for osteogenic differentiation in the 3D cultures system. Considering our Bradford quantification showed high level of total proteins in Day 3 and Day 7 extracts from 3D culture whereas our gene expression analysis only showed basal level *RUNX2* transcript expression at Day 3 and Day 7 of differentiation in 3D culture, we propose that basal level *RUNX2* mRNA expression, just like undifferentiated BM-MSCs, might be a possible cause for not detecting RUNX2 proteins at Day 3 and Day 7 of differentiation.

Osx is another key regulator of osteogenesis, functioning downstream of Runx2 and *Osx* expression is directly modulated by Runx2 (Nakashima et al., 2002) (Nishio et al., 2006). Considering *Osx* expression is contingent upon that of *Runx2* (Nakashima et al., 2002), *Osx* is expected be expressed at early stage of differentiation. From our 2D gene

expression experiment, we have found that compared to control (Day 0), *OSX* expression significantly upregulates at Day 3, showing 13.3 fold increment over control in 2D culture the (Figure 13), supporting existing tenet. However, OSX expression is downregulated at Day 7 about 12-fold, and then continues to express at an equilibrium rate (1.6 fold increment over control) at Day 14 and Day 21.

Surprisingly, in our 3D culture experiment, *OSX* expression is actually downregulated at Day 3 and Day 7 of osteogenesis by about 5 fold and 20 fold respectively. However, starting Day 7 *OSX* expression is upregulated 2.8 fold and 5.4 fold at Day 21 over control. Downregulation of *OSX* at the early stage of differentiation in 3D culture system compared to 2D culture system might be associated with low level of *RUNX2* expression at Day 3 and Day 7 of differentiation in 3D culture system.

Twist is a negative regulator of osteogenesis and previous studies found that Twist expression is repressed during the early phases of osteogenesis, preferably by Runx2 (Lee et al., 1999) (Hayashi et al., 2007). In our 2D culture experiments, we have found that *TWIST* expression is initially upregulated at Day 3 (about 9 fold over control) of differentiation and then down regulates about 2 fold at Day 7 over Day 3(7.9 fold over control) of differentiation. However, *TWIST* expression is repressed at late stage of differentiation marked by basal level expression at Day 14 and Day 21. This observation is consistent with TWIST's function in inhibiting osteogenesis. In our 3D culture system, TWIST expression, however, is downregulated about 1.6 and 2.2 fold at Day 3 and Day 7 of differentiation. Surprisingly TWIST expression returns to basal level expression at Day 14 and Day 21 which suggests that TWIST has a novel expression pattern in 3D system.

Adipogenesis in MSCs or preadipocyte progenitors also proceed as osteogenesis. MSCs or pre-adipocytes received adipogenic stimuli in form of adipogenic Dexamethasone, 3-isobutyl-1-methylxanthine (IBMX), indomethacin, and insulin (Verseijden et al., 2009).

Upon exposure to these differentiation inducers, MSCs or preadipocyte precursors undergoes series of transcriptional and epigenetic remodeling and commit to adipogenic lineage by converting into pre-adipocytes. Upregulation of Erg2, and CREB are very crucial at this stage of lineage commitment (Rosen and MacDougald, 2006; Tang and Lane, 2012). Erg2 and Creb then activates C/EBPβ which is upregulated in preadipocytes, followed by activation of C/EBPγ expression. During terminal differentiation of preadipocytes to mature adipocytes, activated C/EBPβ transactivates C/EBPα, which then activates PPARγ – the master adipogenic regulator (Cristancho and Lazar, 2011). PPARγ and C/EBPα have an inbuilt auto regulatory feedback system where activated PPARγ autoactivates itself as well as C/EBPα. C/EBPα-PPARγ autoregulation continues till the pro-adipocytes differentiate into mature adipocytes. In addition to terminally differentiating into mature adipocytes, both PPARγ and C/EBPα play key role in maintaining mature adipocyte identity (Cristancho and Lazar, 2011; Tang and Lane, 2012).

In our adipogenic differentiation experiments with hBM-MSCs, we have found significant upregulation of *PPARy* expression at Day 3 of differentiation in both 2D and 3D culture system (9.9 fold and 41-fold respectively) while *PPARy* expression significantly downregulated at Day 7 in both systems, with maximum downregulation in 3D culture system. However, *PPARy* is again upregulated at Day 14 and Day 21 of differentiation in both 2D and 3D culture system although such elevation of *PPARy* expression was more

prominent in 2D culture system (Figure 15). Elevated expression of *PPARy* in both 2D and 3D culture suggests increased adipogenesis potential.

In Western blot experiments, we found significantly increased level of PPARy protein at Day 3 of differentiation but not in Day 7 of differentiation which consistent with results from adipogenesis in 3T3-L1 preadipocytes where PPARy proteins were more prominent in Day 3 and 4 but decreased afterwards (Prusty et al., 2002). Surprisingly, in our 3D culture system we did not find noticeable amount of PPARy protein at Day 3, but significantly high amount of PPARy in Day 7 (Figure 18). High PPARy expression at later phase of differentiation in 3D culture system proposes a delay in differentiation process; while hBM-MSCs commits and starts differentiating in 2D culture system, hBM-MSCs in 3D culture system first adopt themselves to the 3D microenvironment, make changes to gene expression and metabolic profile prior to committing to differentiation.

Another possible reason for not observing any expression of PPARγ at Day 7 of differentiation in 2D might be very low level PPARγ which could not be detected by the imaging system or unstable binding of the secondary anybody and subsequent detachment during washing steps.

C/EBPα is another key transcription factor regulating adipogenesis, in particular terminal differentiation of pre-adipocytes to mature adipocytes (Cao et al., 1991; Yeh et al., 1995; Jiang and Lane, 2000). C/EBPα expression is upregulated at the late state of adipogenesis, mostly between Day 5-8 in 3T3-L1 preadipocyte cell line (Cao et al., 1991; Yeh et al., 1995; Jiang and Lane, 2000).

Surprisingly, in our 2D differentiation experiments with hBM-MSCs, C/EBPα expression upregulated about 890 fold at Day 3 of differentiation, but markedly downregulated by 9 fold over control at Day 7 of differentiation (Figure 16). With slight downregulation over Day 7 at Day 14 of differentiation, C/EBPα expression again upregulated at Day 21. Except the early phase of differentiation, C/EBPα expression during the late phase of adipogenic differentiation correlates with that of in preadipocyte cell line. We speculate that high expression C/EBPα during early phase of differentiation in hBM-MSCs may be due to the species-specific difference. Also, high C/EBPα expression in the early phase of differentiation might jump start PPARγ expression for enhanced adipogenesis. Interestingly, C/EBPα expression pattern in our 3D culture system does not correlate with that from 2D culture system. In particular, we have found significant downregulation at Day 3 of differentiation (6.6 fold over control) while C/EBPα continues to be expressed at low level or at basal level throughout the entire differentiation process (Figure 16). Such marked expressional difference of C/EBPα between 2D and 3D culture system could arise from difference in morphology, differentiation capacity, but most importantly global chromatin changes. It would be interestingly to explore how C/EBPβ, an early phase C/EBP transcription factor is expressed during adipogenesis in 3D culture system using qPCR or RNASeq experiments followed by western blot.

CHOP10 is a major negative regulator of adipogenesis that impedes adipogenic differentiation by limiting DNA binding ability of C/EBPβ (Batchvarova et al., 1995; Tang and Lane, 2000). From our 2D gene expression experiments we have found that CHOP10 expression is significantly downregulated at Day 3 of differentiation compared to control (about 3 fold) and remained suppressed throughout the entire differentiation (Figure 17).

This observation is consistent with results by Tang et al., 2000 who found that CHOP10 expression sharply plummets within 24h of differentiation of 3T3-L1 preadipocytes. Our 3D experiments, however, showed different expression pattern of CHOP10; slight increase in CHOP10 expression was found in Day 3 compared to control which downregulated at Day 7. CHOP10 expression increased at Day 14 but returned to basal level expression at Day 21 (Figure 17). Difference in CHOP10 expression between 2D and 3D culture hBM-MSCs differentiation may be associated with change in cell behavior in 3D microenvironment as well as active methylation of *CHOP10* promoter in 3D culture system. It would be interesting to analyze *CHOP10* promoter's DNA methylation level between 2D and 3D culture, using bisulfite sequencing technique.

Another key finding of this study is that besides *OSX* and *C/EBPα,* expression of *RUNX2, TWIST1, PPARγ,* and *CHOP10* is significantly ($p < 0.00001$) lower in undifferentiated hBM-MSCS from 3D culture than undifferentiated hBM-MSCS from 2D culture. In addition to the osteogenic and adipogenic transcription factors, we noticed significantly low-level expression of *GAPDH* transcripts ($p < 0.00001$) in 3D cultured samples compared to the 2D culture system. One of the probable rationales behind low GAPDH expression at mRNA and protein level in 3D culture system over 2D culture system is that hBM-MSCs in 3D PuraMatrix hydrogel might be adapting to stress exerted by the low pH of the matrix and that might affect hBM-MSC's glycolytic activity as well as activating endoplasmic reticulum (ER) stress pathway induced unfolded protein response (UPR) (Sano and Reed, 2013). Also, being able to reorganize the actin cytoskeleton and being able to interact with neighboring BM-MSCs in 3D microenvironment might lead to a new metabolic profile adapted by the 3D cultured BM-

MSCs which may lead to changes in energy metabolism as well as GAPDH expression. It would be interesting to analyze expression of key genes associated ER stress pathway or UPR pathway such ATF4, ATF6, CASR, CHOP, GADD34, IRE1α, JNK, or PERK, in 3D encapsulated undifferentiated hBM-MSCs and compare them to their 2D counterpart (Sano and Reed, 2013). Considering, CHOP is one of the key regulators of ER-UPR stress pathway and play cardinal role in osteogenesis/adipogenesis, we speculate that reduced cell viability and differential gene expression pattern of *GAPDH*, *RUNX2, TWIST1, PPARγ,* and *CHOP10* in 3D cultured BM-MSCs is induced by ER-UPR stress pathway activation via PERK-ATF4-CHOP signaling, during encapsulation of BM-MSCs (Chan et al., 2017; Xu et al., 2017).

Considering our gene expression analysis was done by normalizing expression of each transcription factor to GAPDH expression observed in 2D or 3D culture system and GAPDH expression is relatively lower in 3D culture system than its 2D counterpart, slight difference in expression level of these transcription factors in 3D culture system might be due to the difference in GAPDH expression in 3D. We propose that when analyzing gene expression in PuraMatrix hydrogel based 3D culture, multiple reference or normalizing genes should be analyzed and included in the analysis since GAPDH is not stable across different culture system. In this regard, 18S rRNA and Tata binding protein (TBP) could be potential candidates.

Accumulating evidence corroborates that 3D culture system greatly differs from 2D culture in terms of dimensionality, structure and function of extracellular matrix inside the 3D matrix, and topological effect of the 3D matrix on cell's shape, function and differentiation (Guilak et al., 2009; Lutolf et al., 2009).

In particular, one of the key differences between 2D and 3D culture system is the ability of cells to reorganize themselves and interact with the extracellular matrix more potently due to the increased surface area and dimensionality of the 3D matrix/scaffold. As a result, cells encapsulated or maintained in 3D scaffold/matrix are capable of adopting new morphology/shape. In our study, we have found that BM-MSCs encapsulated in 3D PuraMatrix hydrogel reorganize into spherical shape in contrast to their native spindle shape observed in 2D culture. Interestingly, multiple studies corroborate that the shape of cells plays a substantial role in modulating cells function and differentiation. Using human capillary endothelial cells, Chen et al., (1997) showed that cell survival and apoptosis is largely dependent on cell shape; cellular shapes resulting from limited cell spreading, which is achieved by controlling cell spreading on micropattern surface with different aspect-ratio, coated with ECM proteins, is typically associated with more apoptosis whereas cell shapes resulting from unconstrained spreading, mostly due to large surface area and more opportunity to interact with the ECM, promote cell growth and survival (Chen et al., 1997). Particularly, in hBM-MSCs, cell shape has been found to be a key determinant of MSCs differentiation. By controlling hBM-MSCs shape using micropatterning technique, McBeath et al., (2004) have shown that hMSCs that are unable to spread and adopts round shape undergoes adipogenesis whereas BM-MSCs that adhere, and spread on the surface adopts flattened morphology and preferentially differentiates into osteogenic lineage (McBeath et al., 2004). A similar observation was reported by Kilian et al., (2010) who showed that limited cell spreading promotes adipogenesis while large surface area allowing greater cell spreading promotes osteogenesis (Kilian et al., 2010). Interestingly, McBeath et al., (2004) found that actin-cytoskeleton plays a crucial role in

determining cell shape and lineage commitment. In fact, chemical disruption of actin filament organization or inhibition of myosin generated cytoskeletal tension leads to round cellular shape that promotes adipogenesis and limits osteogenesis and this modulation is directly controlled by RhoA GTPase and Rho kinase (ROCK) (McBeath et al., 2004). In our study, we found that encapsulated hBM-MSCs adopt a round morphology in PuraMatrix based 3D culture. Based on the observations by McBeath et al., (2004) and (Kilian et al., 2010), round shape is indicative of adipogenic differentiation potential. Interestingly, in our gene expression study, we found that in the early stage of differentiation (at Day3), PPARy is significantly increased compared to RUNX2 under adipogenic and osteogenic differentiation condition which might suggests the role of round morphology of 3D encapsulated hBM-MSCs in promoting PPARy expression. It would be interesting to analyze expression of osteogenic and adipogenic transcription factors in 3D encapsulated BM-MSCs without thee differentiation induction over several weeks to validate if round morphology of encapsulated BM-MSCs alone can induce adipogenesis or limit osteogenesis.

Another critical physical property of 3D matrix that directly modulate cells function, viability, and differentiation is matrix stiffness/elasticity (Yang et al., 2017). In addition to regulating cell proliferation, migration, and apoptosis, matrix elasticity/stiffness also regulate stem cell self-renewal and differentiation. For instance, both Engler et al., (2006) and Huebsch et al., (2010) proved that MSCs preferentially undergo osteogenesis when the stiffness of the hydrogel is intermediate to rigid whereas soft matrices favor neurogenic commitment (Engler et al., 2006; Huebsch et al., 2010).

Recent studies have shown that matrix stiffness or elasticity generates mechanical stimuli which are transmitted through integrins and relayed to focal adhesion (FA) kinase (FAK) to activate RhoA and ROCK mediated actomyosin contraction and actin reorganization (McBeath et al., 2004; Lv et al., 2015). Particularly in stiffer substrate which promotes osteogenesis, (Shih et al., 2011), matrix stiffness-induced mechano-transduction increases ROCK, FAK, and ERK1/2 expression which ultimately lead to increased level of RUNX2 expression and osteogenic fate.

In our 3D experiments, we used 0.125% PuraMatrix hydrogel to encapsulate and maintain hBM-MSCs for differentiation. Considering stock PuraMatrix is a 1% hydrogel system, 0.125% represents a much elastic hydrogel. Considering we found significantly increased level of PPARy expression at early stage of differentiation compared to RUNX2 at the same time point of differentiation, we speculate that 0.125% hydrogel may promote adipogenic differentiation over osteogenesis. It would be interesting to analyze osteogenic or adipogenic potential of BM-MSCs maintained in much stiffer hydrogel such as 0.5%, 0.75% or 1% hydrogel.

Conclusion:

In addition to being an excellent platform/model system to study stem cell biology, lineage commitment, and epigenetic/transcriptional gene regulations, mesenchymal stem cells (MSCs) offer unprecedented opportunity in cell-based therapy, tissue engineering, and regenerative medicine, largely owing to MSC's multilineage differentiation potential and immune modulatory property. Many studies are already underway employing MSCs for bone/cartilage repair or bone tissue engineering (Lin et al., 2018), treating cerebral ischemic stroke (CIS) (Ward et al., 2018) and sepsis (Zheng et al., 2018), for liver regeneration (Fiore et al., 2018), to treat primary biliary cholangitis (PBC) (Arsenijevic et al., 2017) and so on.

Despite such remarkable advances in clinical application of MSCs, little progress has been made in uncovering many fundamental aspects of MSC biology such as the transcriptional and epigenetic basis of MSC multipotency and differentiation as well as how tissue origin affects MSCs differentiation and immune-modulation. In particular, MSCs have been found to exhibit substantial cell-to-cell variability within same the same MSC population, between different tissue sources, and between donors (Phinney, 2012; McLeod and Mauck, 2017). Surprisingly, most studies do not account for this inherent heterogeneity of MSCs when analyzing MSCs functionality, differentiation, and immunomodulatory function. Inadequate characterization of multipotent MSCs not only undermines their application in cell-based therapy and regenerative medicine, transplantation of transformed MSCs or MSCs with highly heterogenous genetics background may lead to uncontrolled differentiation, tumor development and cancer metastasis *in vivo* (Chang et al., 2015; Li et al., 2018).

Another major limitation of characterizing different aspects of MSCs biology is the utilization of many different types of MSCs or progenitor cells by different research groups. Historically, differentiation of MSCs into mesodermal lineages such as osteogenic or adipogenic have been studied using murine progenitor cell lines such as MC3T3-E1 preosteoblast cell line or 3T3-L1 pre-adipocyte cell lines (Shao and Lazar, 1997; Xiao et al., 1998). Considering these osteo/adipo progenitor cells are already in a pre-committed developmental stage of differentiation, the molecular mechanisms underlying osteogenesis and adipogenesis from multipotent bona fide MSCs are not truly recapitulated in these cell lines. In fact, in order to translate MSCs into clinical applications, human MSCs should be employed when investigating different aspects of MSCs biology. To this end, hMSCs from hiPSCs or hAD-MSCs (highly convenient to collect) could be a possible source of bona fide multipotent human MSCs.

In this study, we have analyzed osteogenic and adipogenic differentiation of human bone marrow derived mesenchymal stem cells (hBM-MSCs) to characterize gene expression patterns of key osteogenic (RUNX2, OSX, TWIST1) and adipogenic (PPARγ, C/EBPα, CHOP10) transcription factors in human MSCs system. We have found that these transcription factors are dynamically expressed over the course of osteogenic or adipogenic differentiation and their expression pattern in hBM-MSCs differs from that of in pre-osteoblast or pre-adipocyte cell lines. Moreover, we have characterized PuraMatrix peptide hydrogel system for 3D culturing of human BM-MSCs and have compared expression pattern of our defined transcription factors at mRNA and protein level between hBM-MSC maintained in 2D culture and hBM-MSCs encapsulated in a PuraMatrix based 3D culture system. In addition to adopting a novel morphology/shape in 3D culture system, hBM-

MSCs show differential expression of *RUNX2, OSX, TWIST1, PPARγ, C/EBPα,* and *CHOP10* at stages of osteogenic and adipogenic differentiation. Moreover, we speculate that hBM-MSCs encapsulated in 3D culture system might adopt a novel metabolic profile marked by downregulation of GAPDH expression. We propose that compared to conventional 2D culture, a 3D culture system offers more physiological representation of human MSCs.

However, there are certain limitations inherent to studying stem cell differentiation and gene expression analysis in both 2D and 3D culture systems. First of all, induction of differentiation is a stochastic process; despite receiving same differentiation stimuli, only certain fraction of a stem cell population or seeded cells in the cell culture plates commit to differentiation. As a result, there are potential sources of variation between different stem cell populations (biological groups), which may pass onto the analysis of gene/protein expression of target genes and quantification of differentiation using different staining protocols.

In addition, encapsulation of BM-MSCs into PuraMatrix peptide hydrogel, which is a very delicate process, requires high level of meticulousness. PuraMatrix peptide hydrogel is acidic (pH of 2-2.5); therefor, direct contact of cells (suspended in sucrose solution) with the hydrogel results in significant cell death, leading to variable number of viable-cells/wells when encapsulated and seeded in cell culture plates. To minimize cell death, the hydrogel and sucrose-cell suspension should be mixed and plated very quickly followed by immediate gelatination of the gel. Moreover, following encapsulation, the pH of the hydrogel should be calibrated very quickly, by changing the medium multiple times within next the hour.

Also, for analyzing gene expression in 3D culture system, multiple reference genes should be tested and incorporated in the analysis step. We have found that GAPDH, which is a popular reference/housekeeping gene used for normalization in gene expression studies, is differentially expressed in hBM-MSCs when they are maintained in PuraMatrix peptide hydrogel based 3D culture system.

We hope that future studies will focus on overcoming the limitations mentioned above and explore other aspects of human MSC biology and PuraMatrix peptide hydrogel based 3D culture system. In particular, expression of key osteogenic and adipogenic transcription factors should be compared between human MSCs of different tissue origins to validate if tissue origin affects expression pattern of these transcription factors at different stages of differentiation, considering existing report suggests that mouse MSCs of bone marrow origin have an epigenetic predisposition for osteogenic differentiation (Meyer et al., 2016). Time course experimental system in this regard would be very productive in uncovering detailed mechanistic insights into lineage specific gene expression pattern. With regards to PuraMatrix peptide hydrogel based 3D culture system, it would of great interest to compare epigenetic profile, metabolic profile, cell surface markers, and the secretome of MSCs/BM-MSCs maintained in PuraMatrix and other 3D culture system prior to using encapsulated hMSCs for clinical application. High throughput techniques such as RNA-Seq or array based qPCR/PCR would be very productive to perform genome wide analysis study (GWAS) to identify differentially expressed genes in 3D culture hBM-MSCs, followed by their gene ontology analysis.

Further functional characterization of PuraMatrix peptide hydrogel based 3D culture system is essential prior to their application in tissue engineering and clinical

studies. In particular, topological features such as matrix elasticity, porosity, degradation, and mechanical loading should be characterized in PuraMatrix peptide hydrogel since these topological features strongly influence differentiation of MSCs in other hydrogel or 3D culture system (Guilak et al., 2009; Lutolf et al., 2009).

Hopefully, future studies will resolve existing limitations and further character PuraMatrix peptide hydrogel to enable their application in disease/tissue modeling or complex tissue engineering.

References

Adamzyk, C., Kachel, P., Hoss, M., Gremse, F., Modabber, A., Holzle, F., Tolba, R., Neuss, S., and Lethaus, B. (2016). Bone tissue engineering using polyetherketoneketone scaffolds combined with autologous mesenchymal stem cells in a sheep calvarial defect model. J Craniomaxillofac Surg *44*, 985-994.

Arsenijevic, A., Harrell, C.R., Fellabaum, C., and Volarevic, V. (2017). Mesenchymal Stem Cells as New Therapeutic Agents for the Treatment of Primary Biliary Cholangitis. Anal Cell Pathol (Amst) *2017*, 7492836.

Baker, B.M., and Chen, C.S. (2012). Deconstructing the third dimension: how 3D culture microenvironments alter cellular cues. J Cell Sci *125*, 3015-3024.

Bastie, C., Holst, D., Gaillard, D., Jehl-Pietri, C., and Grimaldi, P.A. (1999). Expression of peroxisome proliferator-activated receptor PPARdelta promotes induction of PPARgamma and adipocyte differentiation in 3T3C2 fibroblasts. J Biol Chem *274*, 21920-21925.

Batchvarova, N., Wang, X.Z., and Ron, D. (1995). Inhibition of adipogenesis by the stress-induced protein CHOP (Gadd153). EMBO J *14*, 4654-4661.

Birmingham, E., Niebur, G.L., McHugh, P.E., Shaw, G., Barry, F.P., and McNamara, L.M. (2012). Osteogenic differentiation of mesenchymal stem cells is regulated by osteocyte and osteoblast cells in a simplified bone niche. Eur Cell Mater *23*, 13-27.

Bonaguidi, M.A., Wheeler, M.A., Shapiro, J.S., Stadel, R.P., Sun, G.J., Ming, G.L., and Song, H. (2011). In vivo clonal analysis reveals self-renewing and multipotent adult neural stem cell characteristics. Cell *145*, 1142-1155.

Bonnier, F., Keating, M.E., Wrobel, T.P., Majzner, K., Baranska, M., Garcia-Munoz, A., Blanco, A., and Byrne, H.J. (2015). Cell viability assessment using the Alamar blue assay: a comparison of 2D and 3D cell culture models. Toxicol In Vitro *29*, 124-131.

Bredella, M.A., Torriani, M., Ghomi, R.H., Thomas, B.J., Brick, D.J., Gerweck, A.V., Rosen, C.J., Klibanski, A., and Miller, K.K. (2011). Vertebral bone marrow fat is positively associated with visceral fat and inversely associated with IGF-1 in obese women. Obesity (Silver Spring) *19*, 49-53.

Bruderer, M., Richards, R.G., Alini, M., and Stoddart, M.J. (2014). Role and regulation of RUNX2 in osteogenesis. Eur Cell Mater *28*, 269-286.

Calvi, L.M., Adams, G.B., Weibrecht, K.W., Weber, J.M., Olson, D.P., Knight, M.C., Martin, R.P., Schipani, E., Divieti, P., Bringhurst, F.R., *et al.* (2003). Osteoblastic cells regulate the haematopoietic stem cell niche. Nature *425*, 841-846.

Cao, Z., Umek, R.M., and McKnight, S.L. (1991). Regulated expression of three C/EBP isoforms during adipose conversion of 3T3-L1 cells. Genes Dev *5*, 1538-1552.

Castren, E., Sillat, T., Oja, S., Noro, A., Laitinen, A., Konttinen, Y.T., Lehenkari, P., Hukkanen, M., and Korhonen, M. (2015). Osteogenic differentiation of mesenchymal stromal cells in two-dimensional and three-dimensional cultures without animal serum. Stem Cell Res Ther *6*, 167.

Chan, S.M.H., Zhao, X., Elfowiris, A., Ratnam, C., and Herbert, T.P. (2017). The role of de novo protein synthesis and SIRT1 in ER stress-induced Atf4 and Chop mRNA expression in mammalian cells. Biochimie *138*, 156-167.

Chang, A.I., Schwertschkow, A.H., Nolta, J.A., and Wu, J. (2015). Involvement of mesenchymal stem cells in cancer progression and metastases. Curr Cancer Drug Targets *15*, 88-98.

Chen, C.S., Mrksich, M., Huang, S., Whitesides, G.M., and Ingber, D.E. (1997). Geometric control of cell life and death. Science *276*, 1425-1428.

Chen, Q., Shou, P., Zheng, C., Jiang, M., Cao, G., Yang, Q., Cao, J., Xie, N., Velletri, T., Zhang, X., *et al.* (2016). Fate decision of mesenchymal stem cells: adipocytes or osteoblasts? Cell Death Differ *23*, 1128-1139.

Cheng, S.L., Shao, J.S., Charlton-Kachigian, N., Loewy, A.P., and Towler, D.A. (2003). MSX2 promotes osteogenesis and suppresses adipogenic differentiation of multipotent mesenchymal progenitors. J Biol Chem *278*, 45969-45977.

Chivu, M., Dima, S.O., Stancu, C.I., Dobrea, C., Uscatescu, V., Necula, L.G., Bleotu, C., Tanase, C., Albulescu, R., Ardeleanu, C., *et al.* (2009). In vitro hepatic differentiation of human bone marrow mesenchymal stem cells under differential exposure to liver-specific factors. Transl Res *154*, 122-132.

Corcione, A., Benvenuto, F., Ferretti, E., Giunti, D., Cappiello, V., Cazzanti, F., Risso, M., Gualandi, F., Mancardi, G.L., Pistoia, V., *et al.* (2006). Human mesenchymal stem cells modulate B-cell functions. Blood *107*, 367-372.

Cristancho, A.G., and Lazar, M.A. (2011). Forming functional fat: a growing understanding of adipocyte differentiation. Nat Rev Mol Cell Biol *12*, 722-734.

da Silva Meirelles, L., Chagastelles, P.C., and Nardi, N.B. (2006). Mesenchymal stem cells reside in virtually all post-natal organs and tissues. J Cell Sci *119*, 2204-2213.

De Ugarte, D.A., Morizono, K., Elbarbary, A., Alfonso, Z., Zuk, P.A., Zhu, M., Dragoo, J.L., Ashjian, P., Thomas, B., Benhaim, P., *et al.* (2003). Comparison of multi-lineage cells from human adipose tissue and bone marrow. Cells Tissues Organs *174*, 101-109.

Di Nicola, M., Carlo-Stella, C., Magni, M., Milanesi, M., Longoni, P.D., Matteucci, P., Grisanti, S., and Gianni, A.M. (2002). Human bone marrow stromal cells suppress T-lymphocyte proliferation induced by cellular or nonspecific mitogenic stimuli. Blood *99*, 3838-3843.

Dodig, M., Tadic, T., Kronenberg, M.S., Dacic, S., Liu, Y.H., Maxson, R., Rowe, D.W., and Lichtler, A.C. (1999). Ectopic Msx2 overexpression inhibits and Msx2 antisense stimulates calvarial osteoblast differentiation. Dev Biol *209*, 298-307.

Dominici, M., Le Blanc, K., Mueller, I., Slaper-Cortenbach, I., Marini, F., Krause, D., Deans, R., Keating, A., Prockop, D., and Horwitz, E. (2006). Minimal criteria for defining multipotent mesenchymal stromal cells. The International Society for Cellular Therapy position statement. Cytotherapy *8*, 315-317.

Ducy, P., Zhang, R., Geoffroy, V., Ridall, A.L., and Karsenty, G. (1997). Osf2/Cbfa1: a transcriptional activator of osteoblast differentiation. Cell *89*, 747-754.

Duval, K., Grover, H., Han, L.H., Mou, Y., Pegoraro, A.F., Fredberg, J., and Chen, Z. (2017). Modeling Physiological Events in 2D vs. 3D Cell Culture. Physiology (Bethesda) *32*, 266-277.

Engler, A.J., Sen, S., Sweeney, H.L., and Discher, D.E. (2006). Matrix elasticity directs stem cell lineage specification. Cell *126*, 677-689.

Fajas, L., Schoonjans, K., Gelman, L., Kim, J.B., Najib, J., Martin, G., Fruchart, J.C., Briggs, M., Spiegelman, B.M., and Auwerx, J. (1999). Regulation of peroxisome

proliferator-activated receptor gamma expression by adipocyte differentiation and determination factor 1/sterol regulatory element binding protein 1: implications for adipocyte differentiation and metabolism. Mol Cell Biol *19*, 5495-5503.

Fakhry, M., Hamade, E., Badran, B., Buchet, R., and Magne, D. (2013). Molecular mechanisms of mesenchymal stem cell differentiation towards osteoblasts. World J Stem Cells *5*, 136-148.

Farmer, S.R. (2006). Transcriptional control of adipocyte formation. Cell Metab *4*, 263-273.

Fiore, E.J., Dominguez, L.M., Bayo, J., Garcia, M.G., and Mazzolini, G.D. (2018). Taking advantage of the potential of mesenchymal stromal cells in liver regeneration: Cells and extracellular vesicles as therapeutic strategies. World J Gastroenterol *24*, 2427-2440.

Gauvin, R., Chen, Y.C., Lee, J.W., Soman, P., Zorlutuna, P., Nichol, J.W., Bae, H., Chen, S., and Khademhosseini, A. (2012). Microfabrication of complex porous tissue engineering scaffolds using 3D projection stereolithography. Biomaterials *33*, 3824-3834.

Gonzalez, M.A., and Bernad, A. (2012). Characteristics of adult stem cells. Adv Exp Med Biol *741*, 103-120.

Grandel, H., Kaslin, J., Ganz, J., Wenzel, I., and Brand, M. (2006). Neural stem cells and neurogenesis in the adult zebrafish brain: origin, proliferation dynamics, migration and cell fate. Dev Biol *295*, 263-277.

Guilak, F., Cohen, D.M., Estes, B.T., Gimble, J.M., Liedtke, W., and Chen, C.S. (2009). Control of stem cell fate by physical interactions with the extracellular matrix. Cell Stem Cell *5*, 17-26.

Guo, L., Zhao, R.C., and Wu, Y. (2011). The role of microRNAs in self-renewal and differentiation of mesenchymal stem cells. Exp Hematol *39*, 608-616.

Hamm, J.K., Park, B.H., and Farmer, S.R. (2001). A role for C/EBPbeta in regulating peroxisome proliferator-activated receptor gamma activity during adipogenesis in 3T3-L1 preadipocytes. J Biol Chem *276*, 18464-18471.

Hassan, M.Q., Javed, A., Morasso, M.I., Karlin, J., Montecino, M., van Wijnen, A.J., Stein, G.S., Stein, J.L., and Lian, J.B. (2004). Dlx3 transcriptional regulation of osteoblast differentiation: temporal recruitment of Msx2, Dlx3, and Dlx5 homeodomain proteins to chromatin of the osteocalcin gene. Mol Cell Biol *24*, 9248-9261.

Hassan, M.Q., Tare, R.S., Lee, S.H., Mandeville, M., Morasso, M.I., Javed, A., van Wijnen, A.J., Stein, J.L., Stein, G.S., and Lian, J.B. (2006). BMP2 commitment to the osteogenic lineage involves activation of Runx2 by DLX3 and a homeodomain transcriptional network. J Biol Chem *281*, 40515-40526.

Hayashi, M., Nimura, K., Kashiwagi, K., Harada, T., Takaoka, K., Kato, H., Tamai, K., and Kaneda, Y. (2007). Comparative roles of Twist-1 and Id1 in transcriptional regulation by BMP signaling. J Cell Sci *120*, 1350-1357.

Hishida, T., Nishizuka, M., Osada, S., and Imagawa, M. (2009). The role of C/EBPdelta in the early stages of adipogenesis. Biochimie *91*, 654-657.

Holmes, T.C., de Lacalle, S., Su, X., Liu, G., Rich, A., and Zhang, S. (2000). Extensive neurite outgrowth and active synapse formation on self-assembling peptide scaffolds. Proc Natl Acad Sci U S A *97*, 6728-6733.

Hu, E., Tontonoz, P., and Spiegelman, B.M. (1995). Transdifferentiation of myoblasts by the adipogenic transcription factors PPAR gamma and C/EBP alpha. Proc Natl Acad Sci U S A *92*, 9856-9860.

Huebsch, N., Arany, P.R., Mao, A.S., Shvartsman, D., Ali, O.A., Bencherif, S.A., Rivera-Feliciano, J., and Mooney, D.J. (2010). Harnessing traction-mediated manipulation of the cell/matrix interface to control stem-cell fate. Nat Mater *9*, 518-526.

Ichida, F., Nishimura, R., Hata, K., Matsubara, T., Ikeda, F., Hisada, K., Yatani, H., Cao, X., Komori, T., Yamaguchi, A., *et al.* (2004). Reciprocal roles of MSX2 in regulation of osteoblast and adipocyte differentiation. J Biol Chem *279*, 34015-34022.

Javed, A., Chen, H., and Ghori, F.Y. (2010). Genetic and transcriptional control of bone formation. Oral Maxillofac Surg Clin North Am *22*, 283-293, v.

Jiang, M.S., and Lane, M.D. (2000). Sequential repression and activation of the CCAAT enhancer-binding protein-alpha (C/EBPalpha) gene during adipogenesis. Proc Natl Acad Sci U S A *97*, 12519-12523.

Justesen, J., Stenderup, K., Ebbesen, E.N., Mosekilde, L., Steiniche, T., and Kassem, M. (2001). Adipocyte tissue volume in bone marrow is increased with aging and in patients with osteoporosis. Biogerontology *2*, 165-171.

Kaltz, N., Ringe, J., Holzwarth, C., Charbord, P., Niemeyer, M., Jacobs, V.R., Peschel, C., Haupl, T., and Oostendorp, R.A. (2010). Novel markers of mesenchymal stem cells defined by genome-wide gene expression analysis of stromal cells from different sources. Exp Cell Res *316*, 2609-2617.

Kang, S., Bennett, C.N., Gerin, I., Rapp, L.A., Hankenson, K.D., and Macdougald, O.A. (2007). Wnt signaling stimulates osteoblastogenesis of mesenchymal precursors by

suppressing CCAAT/enhancer-binding protein alpha and peroxisome proliferator-activated receptor gamma. J Biol Chem *282*, 14515-14524.

Kariminekoo, S., Movassaghpour, A., Rahimzadeh, A., Talebi, M., Shamsasenjan, K., and Akbarzadeh, A. (2016). Implications of mesenchymal stem cells in regenerative medicine. Artif Cells Nanomed Biotechnol *44*, 749-757.

Karsenty, G., Kronenberg, H.M., and Settembre, C. (2009). Genetic control of bone formation. Annu Rev Cell Dev Biol *25*, 629-648.

Kilian, K.A., Bugarija, B., Lahn, B.T., and Mrksich, M. (2010). Geometric cues for directing the differentiation of mesenchymal stem cells. Proc Natl Acad Sci U S A *107*, 4872-4877.

Kim, J.B., and Spiegelman, B.M. (1996). ADD1/SREBP1 promotes adipocyte differentiation and gene expression linked to fatty acid metabolism. Genes Dev *10*, 1096-1107.

Kim, S.H., Cho, K.W., Choi, H.S., Park, S.J., Rhee, Y., Jung, H.S., and Lim, S.K. (2009). The forkhead transcription factor Foxc2 stimulates osteoblast differentiation. Biochem Biophys Res Commun *386*, 532-536.

Kobayashi, H., Gao, Y., Ueta, C., Yamaguchi, A., and Komori, T. (2000). Multilineage differentiation of Cbfa1-deficient calvarial cells in vitro. Biochem Biophys Res Commun *273*, 630-636.

Kokabu, S., Nguyen, T., Ohte, S., Sato, T., Katagiri, T., Yoda, T., and Rosen, V. (2013). TLE3, transducing-like enhancer of split 3, suppresses osteoblast differentiation of bone marrow stromal cells. Biochem Biophys Res Commun *438*, 205-210.

Komori, T. (2006). Regulation of osteoblast differentiation by transcription factors. J Cell Biochem *99*, 1233-1239.

Komori, T. (2010). Regulation of bone development and extracellular matrix protein genes by RUNX2. Cell Tissue Res *339*, 189-195.

Komori, T., Yagi, H., Nomura, S., Yamaguchi, A., Sasaki, K., Deguchi, K., Shimizu, Y., Bronson, R.T., Gao, Y.H., Inada, M., *et al.* (1997). Targeted disruption of Cbfa1 results in a complete lack of bone formation owing to maturational arrest of osteoblasts. Cell *89*, 755-764.

Koutsopoulos, S., and Zhang, S. (2013). Long-term three-dimensional neural tissue cultures in functionalized self-assembling peptide hydrogels, matrigel and collagen I. Acta Biomater *9*, 5162-5169.

Kraus, N.A., Ehebauer, F., Zapp, B., Rudolphi, B., Kraus, B.J., and Kraus, D. (2016). Quantitative assessment of adipocyte differentiation in cell culture. Adipocyte *5*, 351-358.

Kurata, H., Guillot, P.V., Chan, J., and Fisk, N.M. (2007). Osterix induces osteogenic gene expression but not differentiation in primary human fetal mesenchymal stem cells. Tissue Eng *13*, 1513-1523.

Le Blanc, K., and Mougiakakos, D. (2012). Multipotent mesenchymal stromal cells and the innate immune system. Nat Rev Immunol *12*, 383-396.

Lee, K.S., Kim, H.J., Li, Q.L., Chi, X.Z., Ueta, C., Komori, T., Wozney, J.M., Kim, E.G., Choi, J.Y., Ryoo, H.M., *et al.* (2000). Runx2 is a common target of transforming growth factor beta1 and bone morphogenetic protein 2, and cooperation between Runx2 and Smad5 induces osteoblast-specific gene expression in the pluripotent mesenchymal precursor cell line C2C12. Mol Cell Biol *20*, 8783-8792.

Lee, M.S., Lowe, G.N., Strong, D.D., Wergedal, J.E., and Glackin, C.A. (1999). TWIST, a basic helix-loop-helix transcription factor, can regulate the human osteogenic lineage. J Cell Biochem *75*, 566-577.

Lee, R.H., Kim, B., Choi, I., Kim, H., Choi, H.S., Suh, K., Bae, Y.C., and Jung, J.S. (2004). Characterization and expression analysis of mesenchymal stem cells from human bone marrow and adipose tissue. Cell Physiol Biochem *14*, 311-324.

Li, C.Y., Wu, X.Y., Tong, J.B., Yang, X.X., Zhao, J.L., Zheng, Q.F., Zhao, G.B., and Ma, Z.J. (2015). Comparative analysis of human mesenchymal stem cells from bone marrow and adipose tissue under xeno-free conditions for cell therapy. Stem Cell Res Ther *6*, 55.

Li, H., Marijanovic, I., Kronenberg, M.S., Erceg, I., Stover, M.L., Velonis, D., Mina, M., Heinrich, J.G., Harris, S.E., Upholt, W.B., *et al.* (2008). Expression and function of Dlx genes in the osteoblast lineage. Dev Biol *316*, 458-470.

Li, J.H., Fan, W.S., Wang, M.M., Wang, Y.H., and Ren, Z.G. (2018). Effects of mesenchymal stem cells on solid tumor metastasis in experimental cancer models: a systematic review and meta-analysis. J Transl Med *16*, 113.

Lin, H., Sohn, J., Shen, H., Langhans, M.T., and Tuan, R.S. (2018). Bone marrow mesenchymal stem cells: Aging and tissue engineering applications to enhance bone healing. Biomaterials.

Livak, K.J., and Schmittgen, T.D. (2001). Analysis of relative gene expression data using real-time quantitative PCR and the 2(-Delta Delta C(T)) Method. Methods *25*, 402-408.

Lutolf, M.P., Gilbert, P.M., and Blau, H.M. (2009). Designing materials to direct stem-cell fate. Nature *462*, 433-441.

Lv, H., Li, L., Sun, M., Zhang, Y., Chen, L., Rong, Y., and Li, Y. (2015). Mechanism of regulation of stem cell differentiation by matrix stiffness. Stem Cell Res Ther *6*, 103.

McBeath, R., Pirone, D.M., Nelson, C.M., Bhadriraju, K., and Chen, C.S. (2004). Cell shape, cytoskeletal tension, and RhoA regulate stem cell lineage commitment. Dev Cell *6*, 483-495.

McLeod, C.M., and Mauck, R.L. (2017). On the origin and impact of mesenchymal stem cell heterogeneity: new insights and emerging tools for single cell analysis. Eur Cell Mater *34*, 217-231.

Mendez-Ferrer, S., Michurina, T.V., Ferraro, F., Mazloom, A.R., Macarthur, B.D., Lira, S.A., Scadden, D.T., Ma'ayan, A., Enikolopov, G.N., and Frenette, P.S. (2010). Mesenchymal and haematopoietic stem cells form a unique bone marrow niche. Nature *466*, 829-834.

Meyer, M.B., Benkusky, N.A., Sen, B., Rubin, J., and Pike, J.W. (2016). Epigenetic Plasticity Drives Adipogenic and Osteogenic Differentiation of Marrow-derived Mesenchymal Stem Cells. J Biol Chem *291*, 17829-17847.

Moerman, E.J., Teng, K., Lipschitz, D.A., and Lecka-Czernik, B. (2004). Aging activates adipogenic and suppresses osteogenic programs in mesenchymal marrow stroma/stem cells: the role of PPAR-gamma2 transcription factor and TGF-beta/BMP signaling pathways. Aging Cell *3*, 379-389.

Mori, T., Sakaue, H., Iguchi, H., Gomi, H., Okada, Y., Takashima, Y., Nakamura, K., Nakamura, T., Yamauchi, T., Kubota, N., *et al.* (2005). Role of Kruppel-like factor 15 (KLF15) in transcriptional regulation of adipogenesis. J Biol Chem *280*, 12867-12875.

Mota de Sa, P., Richard, A.J., Hang, H., and Stephens, J.M. (2017). Transcriptional Regulation of Adipogenesis. Compr Physiol *7*, 635-674.

Nakashima, K., Zhou, X., Kunkel, G., Zhang, Z., Deng, J.M., Behringer, R.R., and de Crombrugghe, B. (2002). The novel zinc finger-containing transcription factor osterix is required for osteoblast differentiation and bone formation. Cell *108*, 17-29.

Narmoneva, D.A., Oni, O., Sieminski, A.L., Zhang, S., Gertler, J.P., Kamm, R.D., and Lee, R.T. (2005). Self-assembling short oligopeptides and the promotion of angiogenesis. Biomaterials *26*, 4837-4846.

Nauta, A.J., Kruisselbrink, A.B., Lurvink, E., Willemze, R., and Fibbe, W.E. (2006). Mesenchymal stem cells inhibit generation and function of both CD34+-derived and monocyte-derived dendritic cells. J Immunol *177*, 2080-2087.

Nichols, J., and Smith, A. (2012). Pluripotency in the embryo and in culture. Cold Spring Harb Perspect Biol *4*, a008128.

Nishio, Y., Dong, Y., Paris, M., O'Keefe, R.J., Schwarz, E.M., and Drissi, H. (2006). Runx2-mediated regulation of the zinc finger Osterix/Sp7 gene. Gene *372*, 62-70.

Oishi, Y., Manabe, I., Tobe, K., Tsushima, K., Shindo, T., Fujiu, K., Nishimura, G., Maemura, K., Yamauchi, T., Kubota, N., *et al.* (2005). Kruppel-like transcription factor KLF5 is a key regulator of adipocyte differentiation. Cell Metab *1*, 27-39.

Omatsu, Y., Sugiyama, T., Kohara, H., Kondoh, G., Fujii, N., Kohno, K., and Nagasawa, T. (2010). The essential functions of adipo-osteogenic progenitors as the hematopoietic stem and progenitor cell niche. Immunity *33*, 387-399.

Oostendorp, R.A., Harvey, K.N., Kusadasi, N., de Bruijn, M.F., Saris, C., Ploemacher, R.E., Medvinsky, A.L., and Dzierzak, E.A. (2002). Stromal cell lines from mouse aorta-

gonads-mesonephros subregions are potent supporters of hematopoietic stem cell activity. Blood *99*, 1183-1189.

Panepucci, R.A., Siufi, J.L., Silva, W.A., Jr., Proto-Siquiera, R., Neder, L., Orellana, M., Rocha, V., Covas, D.T., and Zago, M.A. (2004). Comparison of gene expression of umbilical cord vein and bone marrow-derived mesenchymal stem cells. Stem Cells *22*, 1263-1278.

Park, S.J., Gadi, J., Cho, K.W., Kim, K.J., Kim, S.H., Jung, H.S., and Lim, S.K. (2011). The forkhead transcription factor Foxc2 promotes osteoblastogenesis via up-regulation of integrin beta1 expression. Bone *49*, 428-438.

Peng, L., Jia, Z., Yin, X., Zhang, X., Liu, Y., Chen, P., Ma, K., and Zhou, C. (2008). Comparative analysis of mesenchymal stem cells from bone marrow, cartilage, and adipose tissue. Stem Cells Dev *17*, 761-773.

Phinney, D.G. (2012). Functional heterogeneity of mesenchymal stem cells: implications for cell therapy. J Cell Biochem *113*, 2806-2812.

Pittenger, M.F. (2008). Mesenchymal stem cells from adult bone marrow. Methods Mol Biol *449*, 27-44.

Pittenger, M.F., Mackay, A.M., Beck, S.C., Jaiswal, R.K., Douglas, R., Mosca, J.D., Moorman, M.A., Simonetti, D.W., Craig, S., and Marshak, D.R. (1999). Multilineage potential of adult human mesenchymal stem cells. Science *284*, 143-147.

Prusty, D., Park, B.H., Davis, K.E., and Farmer, S.R. (2002). Activation of MEK/ERK signaling promotes adipogenesis by enhancing peroxisome proliferator-activated receptor gamma (PPARgamma) and C/EBPalpha gene expression during the differentiation of 3T3-L1 preadipocytes. J Biol Chem *277*, 46226-46232.

Robledo, R.F., Rajan, L., Li, X., and Lufkin, T. (2002). The Dlx5 and Dlx6 homeobox genes are essential for craniofacial, axial, and appendicular skeletal development. Genes Dev *16*, 1089-1101.

Rosen, E.D., Hsu, C.H., Wang, X., Sakai, S., Freeman, M.W., Gonzalez, F.J., and Spiegelman, B.M. (2002). C/EBPalpha induces adipogenesis through PPARgamma: a unified pathway. Genes Dev *16*, 22-26.

Rosen, E.D., and MacDougald, O.A. (2006). Adipocyte differentiation from the inside out. Nat Rev Mol Cell Biol *7*, 885-896.

Ruoslahti, E. (1996). RGD and other recognition sequences for integrins. Annu Rev Cell Dev Biol *12*, 697-715.

Ryoo, H.M., Hoffmann, H.M., Beumer, T., Frenkel, B., Towler, D.A., Stein, G.S., Stein, J.L., van Wijnen, A.J., and Lian, J.B. (1997). Stage-specific expression of Dlx-5 during osteoblast differentiation: involvement in regulation of osteocalcin gene expression. Mol Endocrinol *11*, 1681-1694.

Saidi, N., Ghalavand, M., Hashemzadeh, M.S., Dorostkar, R., Mohammadi, H., and Mahdian-Shakib, A. (2017). Dynamic changes of epigenetic signatures during chondrogenic and adipogenic differentiation of mesenchymal stem cells. Biomed Pharmacother *89*, 719-731.

Sano, R., and Reed, J.C. (2013). ER stress-induced cell death mechanisms. Biochim Biophys Acta *1833*, 3460-3470.

Semino, C.E., Merok, J.R., Crane, G.G., Panagiotakos, G., and Zhang, S. (2003). Functional differentiation of hepatocyte-like spheroid structures from putative liver progenitor cells in three-dimensional peptide scaffolds. Differentiation *71*, 262-270.

Shao, D., and Lazar, M.A. (1997). Peroxisome proliferator activated receptor gamma, CCAAT/enhancer-binding protein alpha, and cell cycle status regulate the commitment to adipocyte differentiation. J Biol Chem *272*, 21473-21478.

Shih, Y.R., Tseng, K.F., Lai, H.Y., Lin, C.H., and Lee, O.K. (2011). Matrix stiffness regulation of integrin-mediated mechanotransduction during osteogenic differentiation of human mesenchymal stem cells. J Bone Miner Res *26*, 730-738.

Shirakabe, K., Terasawa, K., Miyama, K., Shibuya, H., and Nishida, E. (2001). Regulation of the activity of the transcription factor Runx2 by two homeobox proteins, Msx2 and Dlx5. Genes Cells *6*, 851-856.

Tadic, T., Dodig, M., Erceg, I., Marijanovic, I., Mina, M., Kalajzic, Z., Velonis, D., Kronenberg, M.S., Kosher, R.A., Ferrari, D., *et al.* (2002). Overexpression of Dlx5 in chicken calvarial cells accelerates osteoblastic differentiation. J Bone Miner Res *17*, 1008-1014.

Tang, Q.Q., and Lane, M.D. (2000). Role of C/EBP homologous protein (CHOP-10) in the programmed activation of CCAAT/enhancer-binding protein-beta during adipogenesis. Proc Natl Acad Sci U S A *97*, 12446-12450.

Tang, Q.Q., and Lane, M.D. (2012). Adipogenesis: from stem cell to adipocyte. Annu Rev Biochem *81*, 715-736.

Tang, Q.Q., Zhang, J.W., and Daniel Lane, M. (2004). Sequential gene promoter interactions by C/EBPbeta, C/EBPalpha, and PPARgamma during adipogenesis. Biochem Biophys Res Commun *318*, 213-218.

Tao, H., Rao, R., and Ma, D.D. (2005). Cytokine-induced stable neuronal differentiation of human bone marrow mesenchymal stem cells in a serum/feeder cell-free condition. Dev Growth Differ *47*, 423-433.

Thomson, J.A., Itskovitz-Eldor, J., Shapiro, S.S., Waknitz, M.A., Swiergiel, J.J., Marshall, V.S., and Jones, J.M. (1998). Embryonic stem cell lines derived from human blastocysts. Science *282*, 1145-1147.

Thonhoff, J.R., Lou, D.I., Jordan, P.M., Zhao, X., and Wu, P. (2008). Compatibility of human fetal neural stem cells with hydrogel biomaterials in vitro. Brain Res *1187*, 42-51.

Tibbitt, M.W., and Anseth, K.S. (2009). Hydrogels as extracellular matrix mimics for 3D cell culture. Biotechnol Bioeng *103*, 655-663.

Tontonoz, P., Hu, E., and Spiegelman, B.M. (1994). Stimulation of adipogenesis in fibroblasts by PPAR gamma 2, a lipid-activated transcription factor. Cell *79*, 1147-1156.

Tontonoz, P., Kim, J.B., Graves, R.A., and Spiegelman, B.M. (1993). ADD1: a novel helix-loop-helix transcription factor associated with adipocyte determination and differentiation. Mol Cell Biol *13*, 4753-4759.

Uccelli, A., Moretta, L., and Pistoia, V. (2008). Mesenchymal stem cells in health and disease. Nat Rev Immunol *8*, 726-736.

Verseijden, F., Jahr, H., Posthumus-van Sluijs, S.J., Ten Hagen, T.L., Hovius, S.E., Seynhaeve, A.L., van Neck, J.W., van Osch, G.J., and Hofer, S.O. (2009). Angiogenic capacity of human adipose-derived stromal cells during adipogenic differentiation: an in vitro study. Tissue Eng Part A *15*, 445-452.

Villanueva, C.J., Waki, H., Godio, C., Nielsen, R., Chou, W.L., Vargas, L., Wroblewski, K., Schmedt, C., Chao, L.C., Boyadjian, R., *et al.* (2011). TLE3 is a dual-function transcriptional coregulator of adipogenesis. Cell Metab *13*, 413-427.

Vining, K.H., and Mooney, D.J. (2017). Mechanical forces direct stem cell behaviour in development and regeneration. Nat Rev Mol Cell Biol *18*, 728-742.

Ward, M.R., Abadeh, A., and Connelly, K.A. (2018). Concise Review: Rational Use of Mesenchymal Stem Cells in the Treatment of Ischemic Heart Disease. Stem Cells Transl Med.

Wilson, A., Laurenti, E., Oser, G., van der Wath, R.C., Blanco-Bose, W., Jaworski, M., Offner, S., Dunant, C.F., Eshkind, L., Bockamp, E., *et al.* (2008). Hematopoietic stem cells reversibly switch from dormancy to self-renewal during homeostasis and repair. Cell *135*, 1118-1129.

Wilson, A., and Trumpp, A. (2006). Bone-marrow haematopoietic-stem-cell niches. Nat Rev Immunol *6*, 93-106.

Witt, R., Weigand, A., Boos, A.M., Cai, A., Dippold, D., Boccaccini, A.R., Schubert, D.W., Hardt, M., Lange, C., Arkudas, A., *et al.* (2017). Mesenchymal stem cells and myoblast differentiation under HGF and IGF-1 stimulation for 3D skeletal muscle tissue engineering. BMC Cell Biol *18*, 15.

Wu, L., Wu, Y., Lin, Y., Jing, W., Nie, X., Qiao, J., Liu, L., Tang, W., and Tian, W. (2007). Osteogenic differentiation of adipose derived stem cells promoted by overexpression of osterix. Mol Cell Biochem *301*, 83-92.

Wu, Z., Xie, Y., Bucher, N.L., and Farmer, S.R. (1995). Conditional ectopic expression of C/EBP beta in NIH-3T3 cells induces PPAR gamma and stimulates adipogenesis. Genes Dev *9*, 2350-2363.

Xiao, G., Wang, D., Benson, M.D., Karsenty, G., and Franceschi, R.T. (1998). Role of the alpha2-integrin in osteoblast-specific gene expression and activation of the Osf2 transcription factor. J Biol Chem *273*, 32988-32994.

Xu, S., Xu, Y., Chen, L., Fang, Q., Song, S., Chen, J., and Teng, J. (2017). RCN1 suppresses ER stress-induced apoptosis via calcium homeostasis and PERK-CHOP signaling. Oncogenesis *6*, e304.

Xu, W., Zhang, X., Qian, H., Zhu, W., Sun, X., Hu, J., Zhou, H., and Chen, Y. (2004). Mesenchymal stem cells from adult human bone marrow differentiate into a cardiomyocyte phenotype in vitro. Exp Biol Med (Maywood) *229*, 623-631.

Yang, Y., Wang, K., Gu, X., and Leong, K.W. (2017). Biophysical Regulation of Cell Behavior-Cross Talk between Substrate Stiffness and Nanotopography. Engineering (Beijing) *3*, 36-54.

Yeh, W.C., Cao, Z., Classon, M., and McKnight, S.L. (1995). Cascade regulation of terminal adipocyte differentiation by three members of the C/EBP family of leucine zipper proteins. Genes Dev *9*, 168-181.

Youngblood, R.L., Truong, N.F., Segura, T., and Shea, L.D. (2018). It's All in the Delivery: Designing Hydrogels for Cell and Non-viral Gene Therapies. Mol Ther.

Zhang, N., Lock, J., Sallee, A., and Liu, H. (2015). Magnetic Nanocomposite Hydrogel for Potential Cartilage Tissue Engineering: Synthesis, Characterization, and Cytocompatibility

with Bone Marrow Derived Mesenchymal Stem Cells. ACS Appl Mater Interfaces *7*, 20987-20998.

Zhang, S., Holmes, T.C., DiPersio, C.M., Hynes, R.O., Su, X., and Rich, A. (1995). Self-complementary oligopeptide matrices support mammalian cell attachment. Biomaterials *16*, 1385-1393.

Zhang, Y., Khan, D., Delling, J., and Tobiasch, E. (2012). Mechanisms underlying the osteo- and adipo-differentiation of human mesenchymal stem cells. ScientificWorldJournal *2012*, 793823.

Zhao, G.Q., Zhao, S., Zhou, X., Eberspaecher, H., Solursh, M., and de Crombrugghe, B. (1994). rDlx, a novel distal-less-like homeoprotein is expressed in developing cartilages and discrete neuronal tissues. Dev Biol *164*, 37-51.

Zheng, G., Huang, R., Qiu, G., Ge, M., Wang, J., Shu, Q., and Xu, J. (2018). Mesenchymal stromal cell-derived extracellular vesicles: regenerative and immunomodulatory effects and potential applications in sepsis. Cell Tissue Res.

Zheng, H., Guo, Z., Ma, Q., Jia, H., and Dang, G. (2004). Cbfa1/osf2 transduced bone marrow stromal cells facilitate bone formation in vitro and in vivo. Calcif Tissue Int *74*, 194-203.

Zuk, P.A., Zhu, M., Ashjian, P., De Ugarte, D.A., Huang, J.I., Mizuno, H., Alfonso, Z.C., Fraser, J.K., Benhaim, P., and Hedrick, M.H. (2002). Human adipose tissue is a source of multipotent stem cells. Mol Biol Cell *13*, 4279-4295.